Impact of Load Type on Microgrid Stability

by

Jared P. Monnin

S.B., E.E. M.I.T., 2011

Submitted to the Department of Electrical Engineering

and Computer Science

in Partial Fulfillment of the Requirements for the Degree of

Master of Engineering in Electrical Engineering and Computer Science

at the Massachusetts Institute of Technology

May 2012

Author: _____

Department of Electrical Engineering and Computer Science
May 21, 2012

Certified by: _____

Professor James L. Kirtley, Jr., Thesis Supervisor
May 21, 2012

Accepted by: _____

Professor Dennis M. Freeman, Chairman, Masters of Engineering Thesis Committee

Impact of Load Type on Microgrid Stability
by
Jared P. Monnin

Submitted to the
Department of Electrical Engineering and Computer Science

May 21, 2012

In Partial Fulfillment of the Requirements for the Degree of
Master of Engineering in Electrical Engineering and Computer Science

ABSTRACT

Microgrids show great promise as a means of integrating distributed generation sources into the public grid distribution system. In order to provide uninterrupted, high quality power to local loads, microgrids must have the ability to operate independently of or in parallel with the local utility. Transitioning between independent operation, also called “islanded” operation, and utility-connected operation can induce stability problems in the microgrid, especially when islanding is fault-induced. Software simulation suggests that induction motor loads on the microgrid significantly decrease stability during fault-induced islanding. To validate the software simulations and to investigate the impact of load type on microgrid stability, we have built a hardware system that simulates the operation of a microgrid.

Thesis Supervisor: James L. Kirtley, Jr., Professor of Electrical Engineering

Acknowledgments

I would like to thank Professor James L. Kirtley, Jr., for his advice and guidance throughout the duration of this project. I would also like to thank Michael Zieve, Jorge Elizondo Martinez, Webb Horn, Zhiyong Wang, Gavin Darcey, Mariusz Klos, and Gaurav Singh for working with me on this project.

Table of Contents

List of Figures

1. Introduction

1.1 Distributed Generation

Since the early 20th century, electric power generation and distribution in the United States has been dominated by large, centralized power plants that are often physically distant from the industrial, commercial, and residential loads that rely on the electric grid for power. Over the last few decades, advances in materials and design have led to an increase in distributed generation, i.e., power plants that are much smaller and often much closer to their loads than traditional power plants. As of 2007, there were approximately 12 million distributed generation sources in the United States, with a combined capacity of 200 gigawatts (U.S. Department of Energy 2007). The vast majority of these distributed generation sources are diesel engine-powered back-up generators, but important expansions in distributed generation have been made through the development of photovoltaic cells, fuel cells, microturbines, and wind turbines. Most distributed generation, especially diesel engine generation, is run only during emergency outages of the electric grid; however, recently developed renewable sources like those mentioned above have been developed for continuous duty.

1.2 Microgrids

With a system designed for back-up generation only, the local load is typically disconnected from the electric grid before being powered by a local distributed generator. With continuous duty distributed generation, however, the local loads are typically connected to a bus that can be powered independently of or in parallel with the local utility. Such a system

configuration is called a “microgrid”. Operating under this regime, microgrids have the potential to provide several beneficial services to the electric grid. With the ability to enter islanded operation quickly, microgrids greatly enhance the reliability of the electric power grid from the point of view of their local loads. Furthermore, microgrids can often provide reactive power to the electric grid, helping to support local voltage levels not only for their own local loads but also for nearby loads. With the development and employment of renewable energy sources like photovoltaic modules and wind turbines, microgrids have the potential to reduce carbon emissions from fossil fuel-based centralized generation. Especially in the case of microgrids with photovoltaic modules, microgrids can also reduce peak power demand from the electric grid, improving the reliability of the grid and reducing cost. Lastly, due to their nature of being distributed over a wide physical area, microgrids using distributed generation sources increase the robustness of the electric grid during natural disasters or accidents that might otherwise cause widespread outages in a grid composed only of centralized generation.

2. Software Simulation

As the distributed generators in microgrids grow in size, it becomes increasingly detrimental to shut down the generators during transient faults on the electric grid. Much of the successful implementation of distributed generation in microgrids relies on the ability of the microgrid to transition between islanded operation and grid-connected operation while maintaining system voltage and frequency within acceptable limits. Intentional islanding of the microgrid induces stability problems on the microgrid that must be accounted for; however, fault-induced islanding of the microgrid induces much more significant stability problems.

Figure 1-1 Response of a microgrid to normal islanding and fault-induced islanding. (a) Per-unit system voltage at load terminals. (b) System frequency at load terminals. (Alaboudy, Zeineldin and Kirtley n.d.)

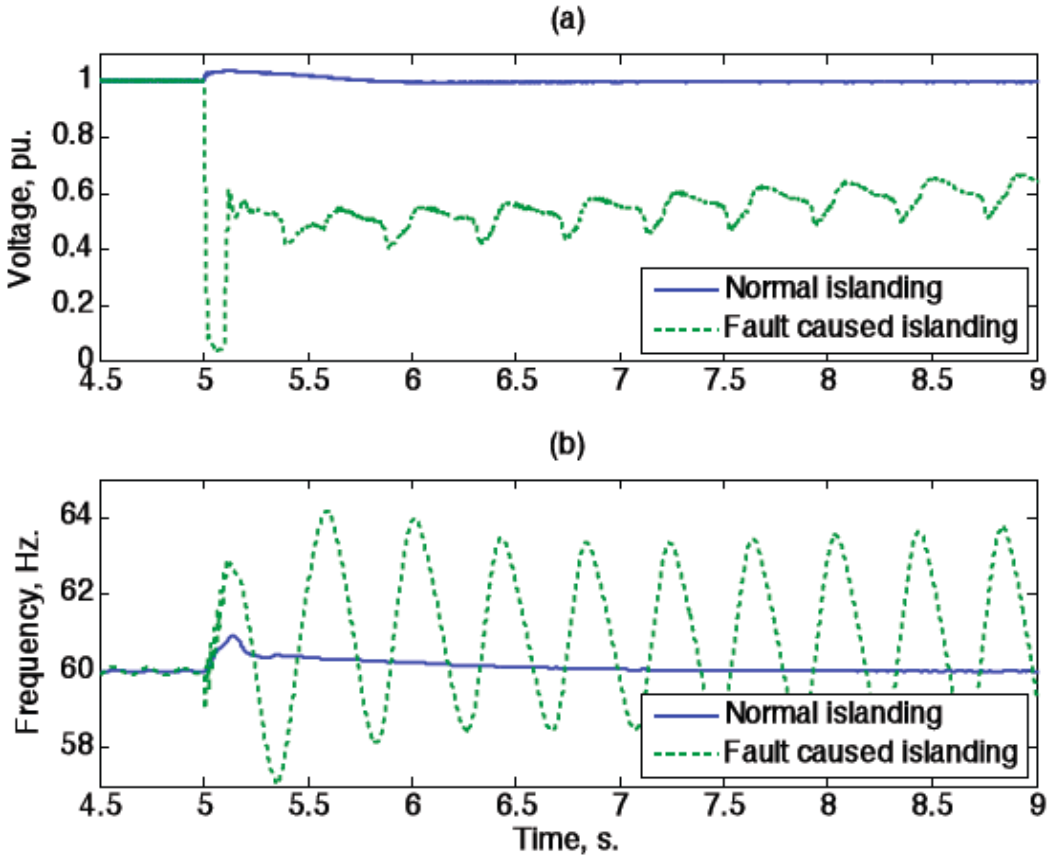

Professors Alaboudy, Zeineldin, and Kirtley used MATLAB/Simulink to develop a model of a typical microgrid system with which they could simulate various operating conditions. Using this model, they found that the response of the system to normal islanding could be much less severe than the response of the system to fault-induced islanding. Investigating fault-induced islanding further, they found that the critical clearing time of the microgrid, which is defined as the duration of time that the distributed generators can withstand a fault and still manage a stable recovery, was heavily influenced by the microgrid control strategy, the distributed

Figure 2-2 One line diagram of Simulink microgrid model. (Alaboudy, Zeineldin and Kirtley n.d.)

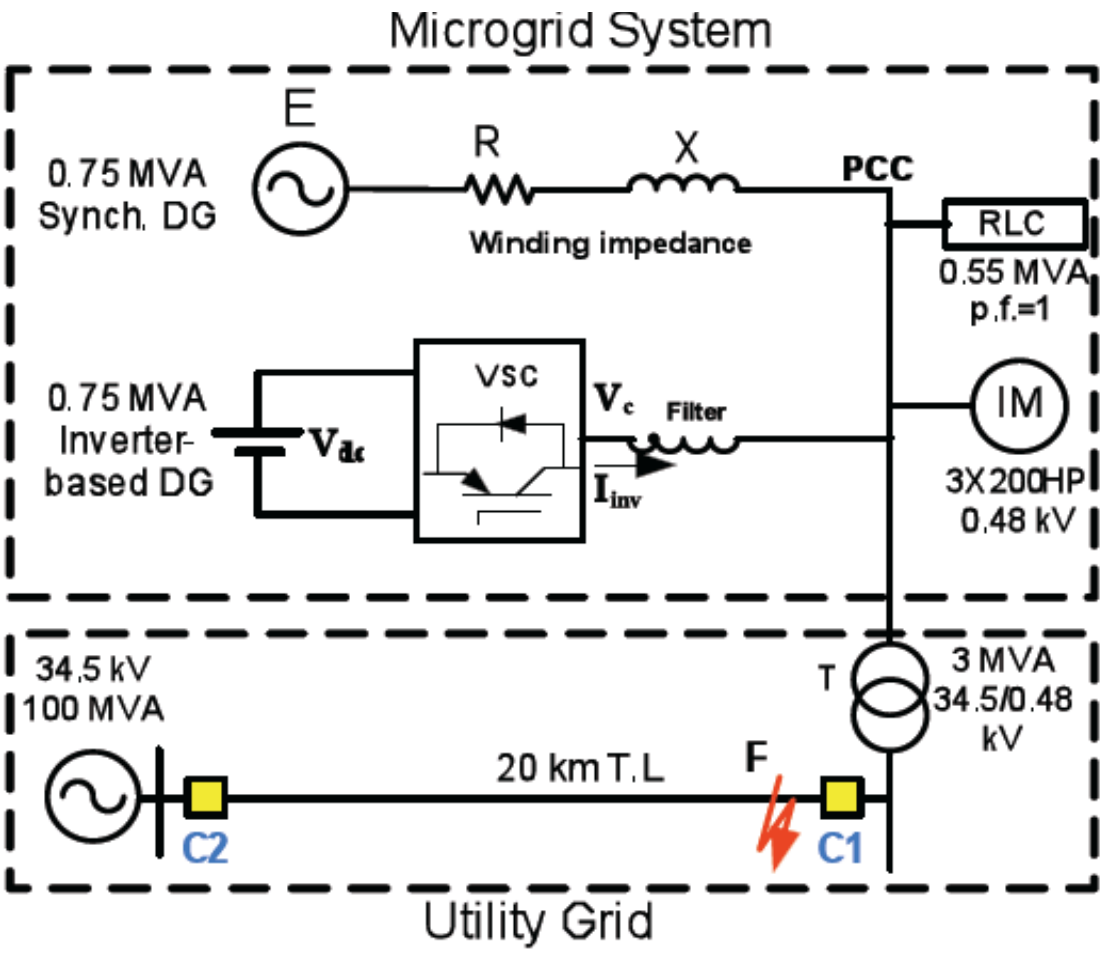

generator control system, and the type of load on the system. In particular, this model demonstrated that induction motor loads have a particularly significant impact on the ability of the distributed generator to recover from a fault. During a fault, the electrical torque on the induction motor shaft is greatly reduced, causing the induction motor shaft speed to decrease and causing the induction motor to draw more reactive power. After the fault is isolated, the microgrid is islanded and attempts to restore system voltage to normal levels, at which point the induction motor will draw large currents from the distributed generator to reaccelerate up to its previous pre-fault speed. This large draw of current and reactive power combine to reduce the ability of the microgrid to recover from a fault into stable islanded operation.

Figure 2-3 Fault-induced islanding recovery near the critical clearing time threshold. (a) Per-unit system voltage at the load terminals. (b) System frequency at the load terminals. (Alaboudy, Zeineldin and Kirtley n.d.)

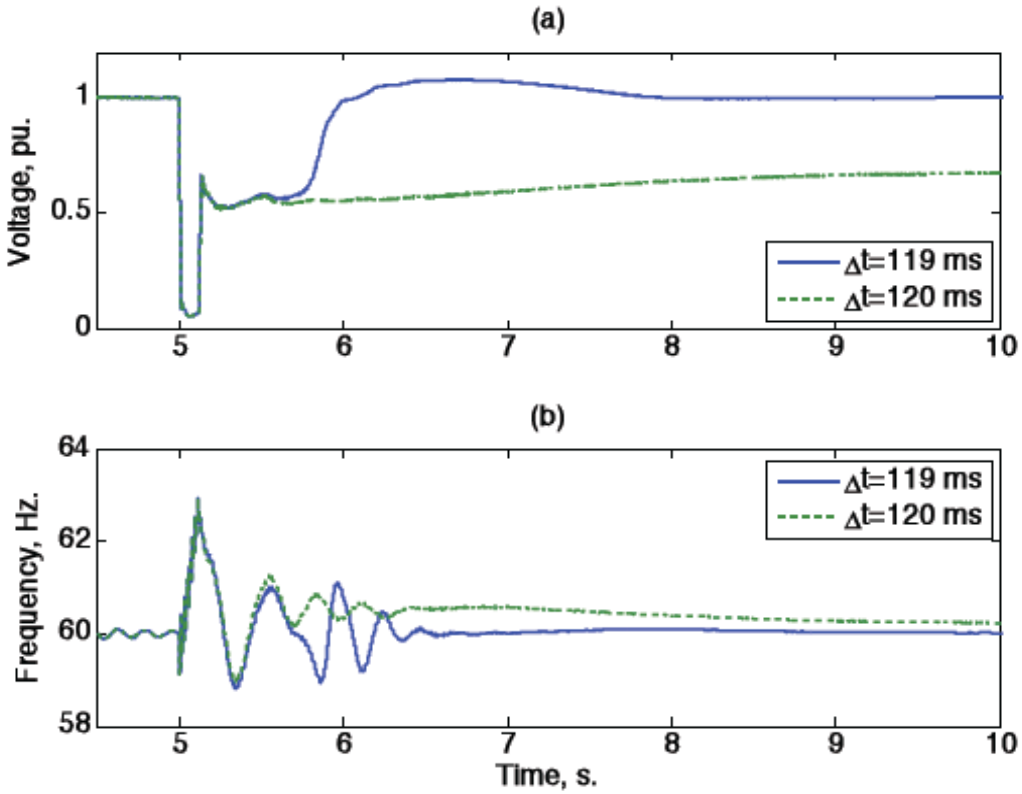

3. Hardware Simulation

3.1 Hardware System Overview

In order to verify the Simulink model of the microgrid system and the results obtained from it, we set out to build a hardware simulation of a microgrid. This system consists of a motor set that emulates a diesel-powered synchronous generator, a set of microinverters that emulate a solar farm, resistive, capacitive, inductive, phase-controlled resistive, and induction motor loads, and a control and measurement system implemented in LabVIEW on our project

Figure 3-1 One line diagram of proposed hardware system.

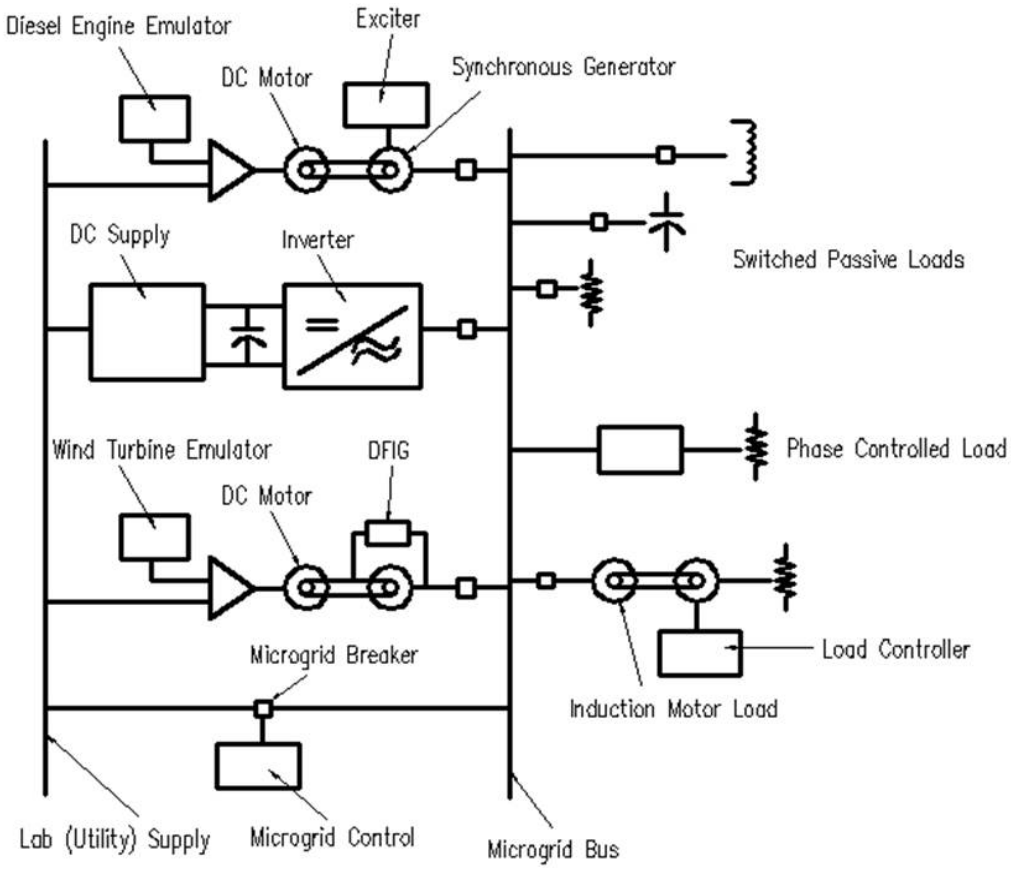

computer. For a detailed description of the hardware system, including descriptions of its construction, operation, and suggestions for future work, see the attached document, Reference Manual for Microgrid Hardware System Simulation.

3.2 Hardware System Simulink Model

In parallel with the construction of the microgrid hardware simulation, I also developed a software model of our hardware system in Simulink. This model simulates most of the components of the physical system, with particular emphasis on the diesel generator system and the induction motor load. We have been able to gain valuable insight from this model that has influenced the design and construction of the hardware model.

3.2.1 Model Overview

The main interface of the Simulink model of our hardware system has a layout very similar to the physical placement of the components on our hardware project board. One of the most important parts of the simulation is the block in the top-left of the interface, called "powergui". This is the environment block for any model containing elements from the SimPowerSystems library and is necessary for the simulation to run. This block stores the equivalent Simulink circuit that represents the state-space equations of the model. Closely related to this block is the Configuration Parameters window, accessible from the Simulation menu on the toolbar. Many of the important parameters of the simulation are set in this window, such as the simulation run time, minimum and maximum time step sizes, and solver type. Most of the interesting transients in this system will happen within 60 seconds and can be captured with a maximum step size of 1/600 seconds, which corresponds to a minimum of ten

steps per cycle at 60 Hz. Choosing a maximum step time larger than this may lead to imprecise waveforms. Choosing the proper solver is also very important. While ode23 and ode45 are the most accurate solvers available, the nonlinear elements of this system prevent these solvers from converging in a reasonable time. Stiff solvers, such as ode15s and ode23tb, are able to converge in a reasonable amount of time, such that a 60-second simulation will finish on the order of minutes, not hours.

Also on the left side of the interface is the clock displaying the present simulation time. Since the solver is set up to use variable minimum time steps, it is possible that the simulation will not run in a reasonable time. While the model can certainly run without this clock displayed, I highly recommend including this clock as it visually displays the size of the time step and will alert the user if Simulink is trying to run a 60-second simulation in nanosecond time steps, which would take an unreasonable amount of time to run.

Starting from the right side of the interface, the lab utility connection is modeled using a three-phase voltage source with 208V phase-to-phase, RMS, at 60 hertz. A large parallel three-phase snubber resistance is included in this subcomponent to help speed up the simulation, but this resistance should have no impact on the rest of the system since the voltage source has no source impedance. The three phases of the utility supply are then connected to a three-phase measurement block that allows us to measure utility voltages, currents, and real and reactive power drawn from the utility.

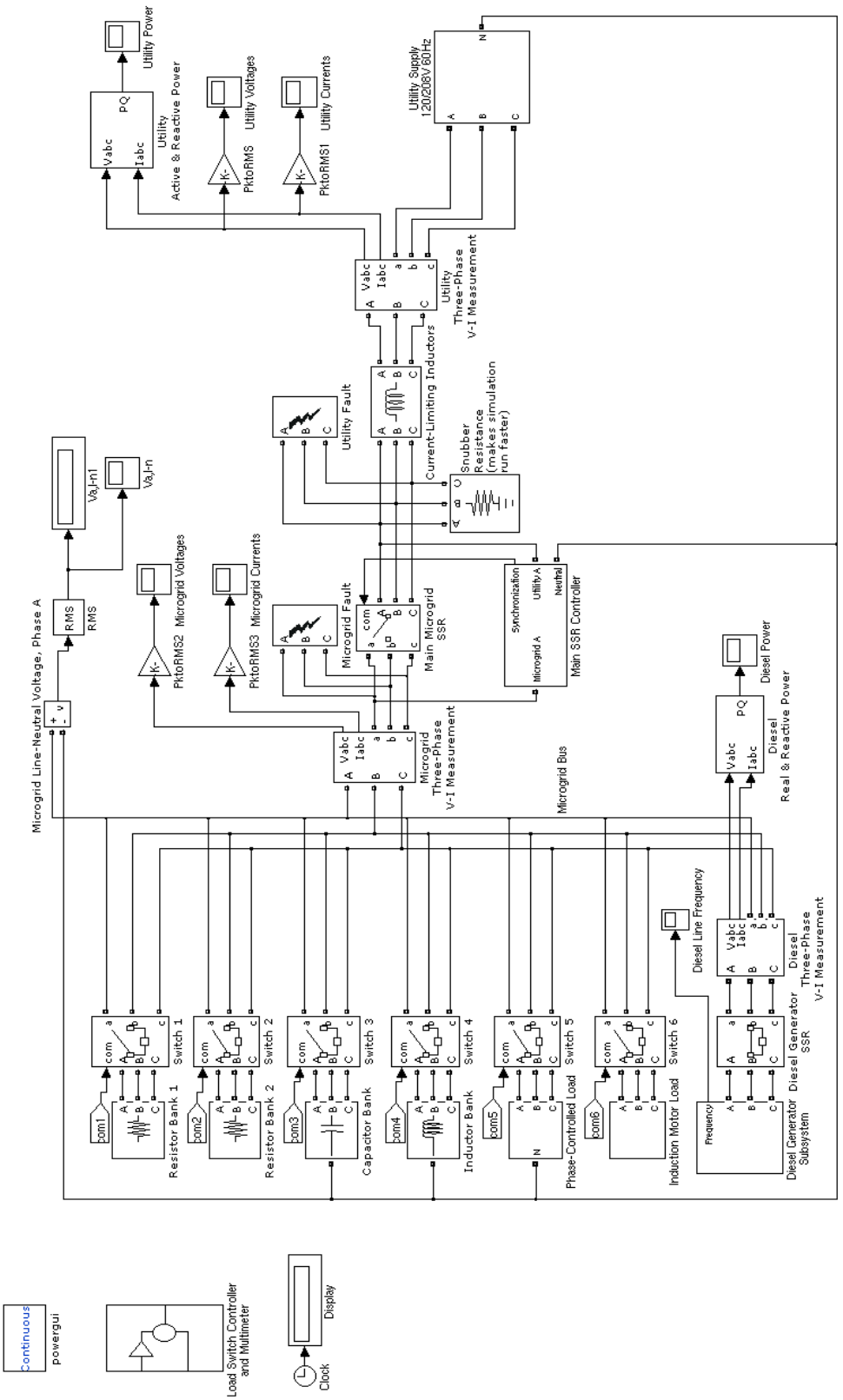

Figure 3-2 Main Interface for Simulink Model of Hardware System

To the left of the utility measurement block is a three-phase series RLC branch block that models our current-limiting inductors. Setting the branch type to “L” makes this block purely inductive. The left terminals of the current-limiting inductors are connected in series with a three-phase switch block that models the main microgrid solid-state relay. Connecting these blocks in this way will raise an error in Simulink because connecting an ideal inductor to an ideal switch will produce singularities in the matrix-solving algorithm. To prevent this error, I introduced a parallel snubber resistance that makes the simulation converge and run faster. Ideally, this parallel resistance should be large to minimize its impact on the system, since it is not a part of the hardware model, but making the resistance too large reduces its ability to speed up the simulation. Also connected between the current-limiting inductors and the main solid-state relay is a block that can simulate a fault on the utility side of the system. The parameters of this block can be adjusted to specify the type of fault induced, as well as the times that the fault turns on and off. Leaving the “transition status” and “transition times” vectors empty is not recommended, and if no change in state is desired, the “transition times” vector should instead be set to a value higher than the length of the simulation run time.

The main microgrid solid-state relay connects the utility supply to the microgrid bus. This three-phase switch can be controlled internally or by an external signal. When controlled internally, the initial status of the breakers must be specified along with a vector of transition times. If no transition is desired, the transition time vector should not be an empty vector but should instead be set to a value higher than the simulation run time. When controlled externally, the initial status of the breakers must still be specified, but transitions are now set

by the external signal transitioning between 0 and 1. I have begun to develop a solid-state relay controller subsystem that would synchronize the utility supply and microgrid bus, but this system has some problems that are not easily resolved without making significant changes to other parts of the system model, specifically the control system of the diesel generator subsystem or the utility supply. The main problem with this subsystem stems from the fact that the frequencies of the utility supply and the diesel generator do not vary once they reach steady state operation, a condition that does not occur in the physical system. Since the frequencies do not change at all, the phase difference between the two systems will never become zero. To enable synchronization in this model, some small random variation in frequency would need to be programmed into the utility supply or the diesel generator model, and I found no simple way to do this.

Connected to the left terminals of the main microgrid solid-state relay is a fault block identical to the fault block on the utility side of the main relay. For a description of the operation of this fault block, see the description of the utility fault block previously in this section. Also connected between the main relay and the microgrid bus is a three-phase measurement block that outputs plots of the microgrid bus voltage and the current through the main microgrid relay. The operation of this block is identical to that of the utility three-phase measurement block.

The microgrid bus connects the utility supply to the diesel generator subsystem and to each of the loads in our model. Each of these elements is connected and disconnected from the microgrid bus by three-phase switches. For each of the load switches, I developed a subsystem,

called Load Switch Controller and Multimeter, which can conveniently set the initial conditions of each switch and measure the voltage across each switch and the current through each switch. Double-clicking on the “manual switches” in this subsystem changes the state of the respective load relay. Double-clicking on the blocks connected to the multimeter block will produce a plot of its respective measurement against time. Note that the default settings of these plotting blocks will plot only the last 5000 data points of the simulation. I changed the parameters of the plotting blocks to plot the full simulation, but newly added blocks will have the default behavior. To change the state of the load switches at different times, the switches must be changed to internal control, where a vector of transition times can be specified.

Figure 3-3 Load Switch Controller and Multimeter Subsystem

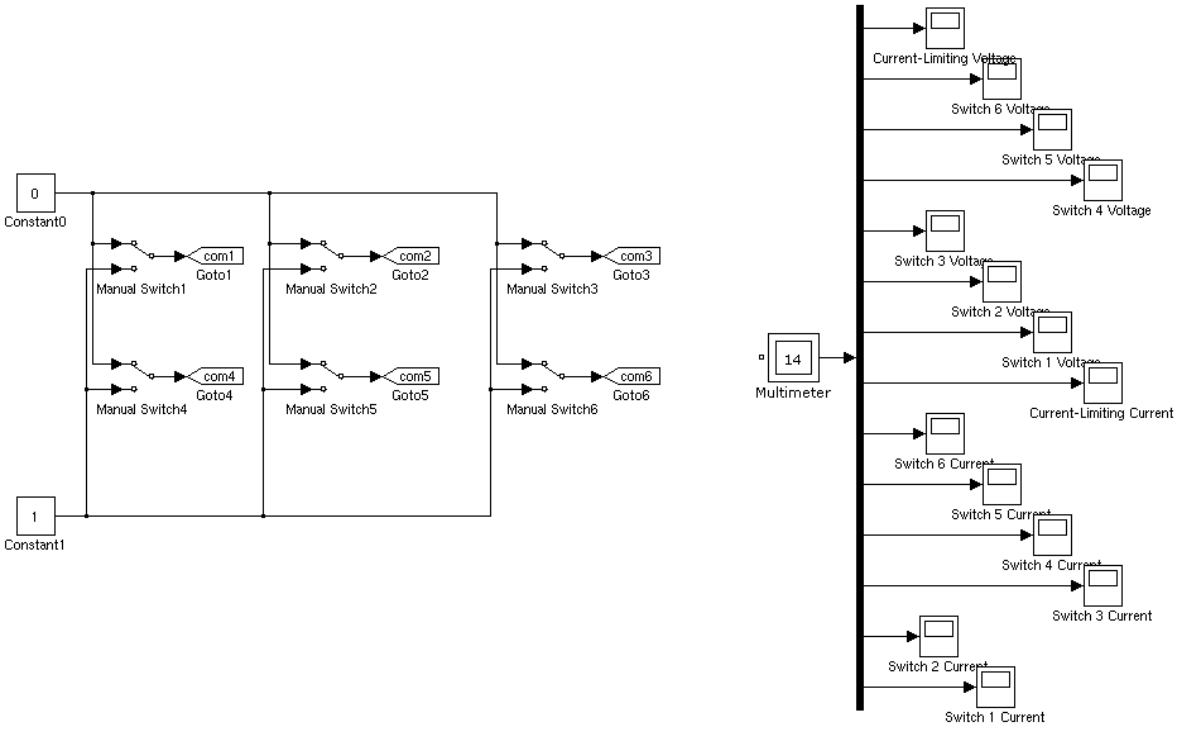

The blocks modeling the resistive, capacitive, and inductive loads are very similar, each being represented with a three-phase series RLC load block. In the parameters of each block, I specified the configuration, either Y with the center point floating in the case of the resistive loads, or Y with the center point connected to neutral in the case of the capacitive and inductive loads. Rather than specifying the values of the circuit elements, this block is described by the type and magnitude of power that it draws. For the purely resistive loads, where each leg of the Y connected circuit contains a 48-ohm resistor, the power is purely real, and is calculated by the equation

$$P = 3 * \frac{(120\ \mathrm{V})^2}{48\ \Omega} = 900\ \mathrm{W}.$$

Similarly for the capacitive and inductive loads, the power is purely reactive and is calculated by the equations

$$Q_C = 3 * \frac{(120\ \mathrm{V})^2}{(2\pi * 60\ \mathrm{Hz} * 44\ \mu\mathrm{F})^{-1}} = 716\ \mathrm{VAR}$$

and

$$Q_L = 3 * \frac{(120\ \mathrm{V})^2}{2\pi\ *\ 60\ \mathrm{Hz}\ * 0.127\ \mathrm{H}} = 900\ \mathrm{VAR}.$$

The phase-controlled resistive load is a simplified model of the actual physical system. Rather than model the full dimmer circuit, I used ideal switches to chop up the phase voltages connected to the 60-watt light bulb array. To generate the gating signals for these switches, I implemented a subsystem that detects the zero crossing of the phase A voltage and triggers a monostable pulse generator. This pulse has an initial duration of 1/120 seconds, half the period

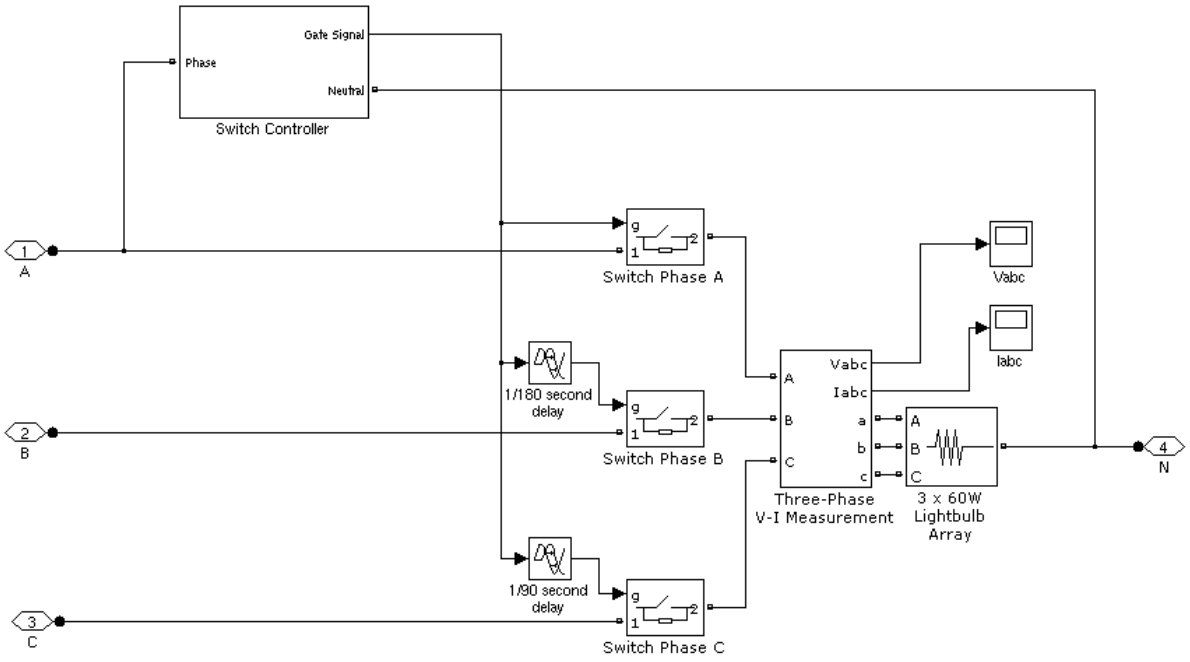

Figure 3-4 Phase-Controlled Resistive Load Subsystem

of a 60-Hz wave, which I then multiply by a complementary percentage that sets the fraction of each sine wave that is cut out. For instance, the present system has a pulse duration of ((100-40)/100)*(1/120) seconds, which means that the first 40% of the voltage sine wave is cut off during each half-cycle. To change this parameter of the phase-controlled load, double-click on the Switch Controller subsystem, and then double-click on the Monostable block to change the percentage to anything between 0 and 100. This gating signal is connected directly to the phase A switch but is delayed by $1/180^{th}$ of a second for the phase B switch and by $1/90^{th}$ of a second for the phase C switch. One drawback of this implementation is that it only gives meaningful results when the system is operating close to 60 hertz.

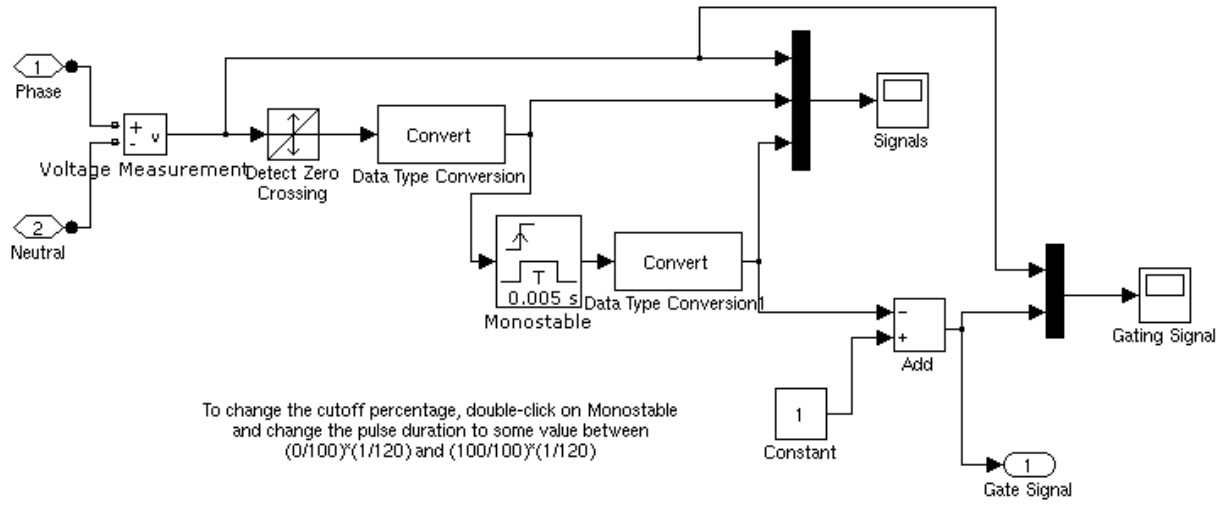

Figure 3-5 Phase-Controlled Resistive Load Gating Signal Subsystem

3.2.2 Induction Motor Load Model

The induction motor load has the most complex model of all the loads. In the physical system, this load consists of a three-phase squirrel-cage induction motor mechanically coupled to a separately-excited DC motor, with the field of the DC motor connected to a voltage source and the armature connected to a power resistor. In the SimPowerSystems models for motors, a motor must have an input signal that specifies either the torque or speed of the motor. Each motor model also has an output signal that consists of a vector of various system variables, such as rotor and stator currents, fluxes, and voltages, and shaft speed, torque, and angle. By setting the squirrel-cage induction motor to take a torque input, setting the DC motor to take a speed input, and then connecting the torque output of the DC motor to the induction motor torque input and connecting the speed output of the induction motor to the DC motor speed input, it is possible to effectively simulate the shafts of the motors being perfectly connected. It

is important to note that the sign of the torque output of the DC motor must be flipped, or else the system will be exponentially unstable.

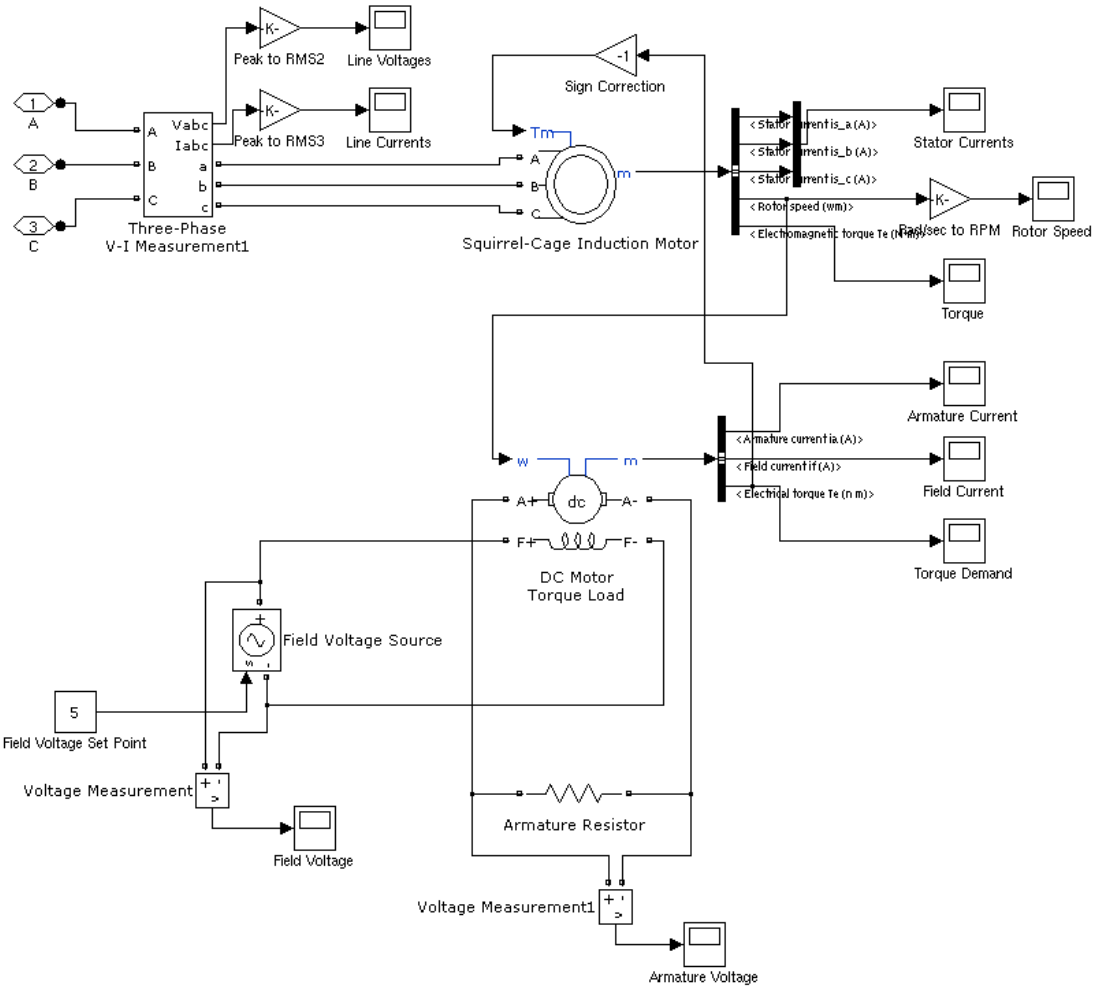

Figure 3-6 Induction Motor Load Subsystem

Once the machines were mechanically coupled, I connected the terminals of the induction motor to the three phases of the microgrid bus through a three-phase measurement block. For the DC motor, I connected the armature to a resistor and connected the field to a controlled voltage source. This voltage source is set by a “constant” block, which commands a constant voltage on the field. To increase the power dissipated by the DC motor and thereby

increase the torque load on the induction motor, simply increase the value of the “constant” block to command a higher voltage on the field of the DC motor. If a specific load profile were desired, it would be very easy to replace this “constant” block with a function builder block that implements the desired load profile.

Double-clicking on the machine models opens up the interface to set the machine type and machine parameters. For this simulation, these parameters were set to the values of the physical machines, which I found using the testing standards outlined in IEEE Standard 112 and IEEE Standard 113. Taking advantage of the output vectors of the machine, I included several plotting blocks to display the stator and rotor currents and voltages of both machines and the rotor speed of the machine set.

3.2.3 Diesel Generator Model

The diesel generator subsystem is the most complex subsystem in the microgrid model and can be divided into two parts: the DC motor and its control system, and the wound-rotor induction motor and its control system. In the physical system, these two motors have their shafts mechanically coupled. To represent this physical coupling, I connected the torque and speed inputs and outputs of the machines in an identical way to that of the induction motor load described in the previous subsection.

The DC motor is the prime mover in this generator set. The field of the DC motor is connected to a constant voltage source of 200 volts DC, which is then connected to a shorted resistor. Since this resistor is shorted, it has no impact on the results of the simulation, but it is necessary to prevent the connection of an ideal inductor to an ideal voltage source, which

causes singularities in the matrix solver. The system connected to the armature of the DC motor is more complex. The overall goal of this control system is to implement the transfer function,

$$\Delta\omega \rightarrow \left[\frac{-0.2s-1}{0.01*0.02s^2+0.01s+1}\right] \rightarrow \left[\frac{40*0.25s+40}{0.009*0.0384s^3+(0.009+0.0384)s^2+s}\right] \rightarrow [e^{-0.024s}] \rightarrow \mathrm{T}_{command},$$

which describes the response of a large diesel engine to changes in shaft speed. The actual implementation of this transfer function is not quite correct, since the original transfer function limits the output of the second block. To the best of my knowledge, there is no way to limit the output of the Simulink transfer function block, so I attempted to implement a subsystem that would take the output of the second transfer function block and only output a clipped version of its input. This had some success, but the block did not limit the integral wind-up of the previous block, so it was not clear whether it was effective in correcting the transfer function or whether it just implemented a different error.

The input to the diesel control subsystem is derived from taking the difference between the motor shaft speed and a set point of 1800 RPM. The output of this transfer function is a commanded torque for the motor, which I subtracted from the actual motor torque and then fed to a PID controller that sets the voltage on the armature of the DC motor. The parameters of this PID controller have a very significant influence over the stability of the DC motor, and much of the time spent on this subsystem was spent adjusting these parameters to achieve stable operation.

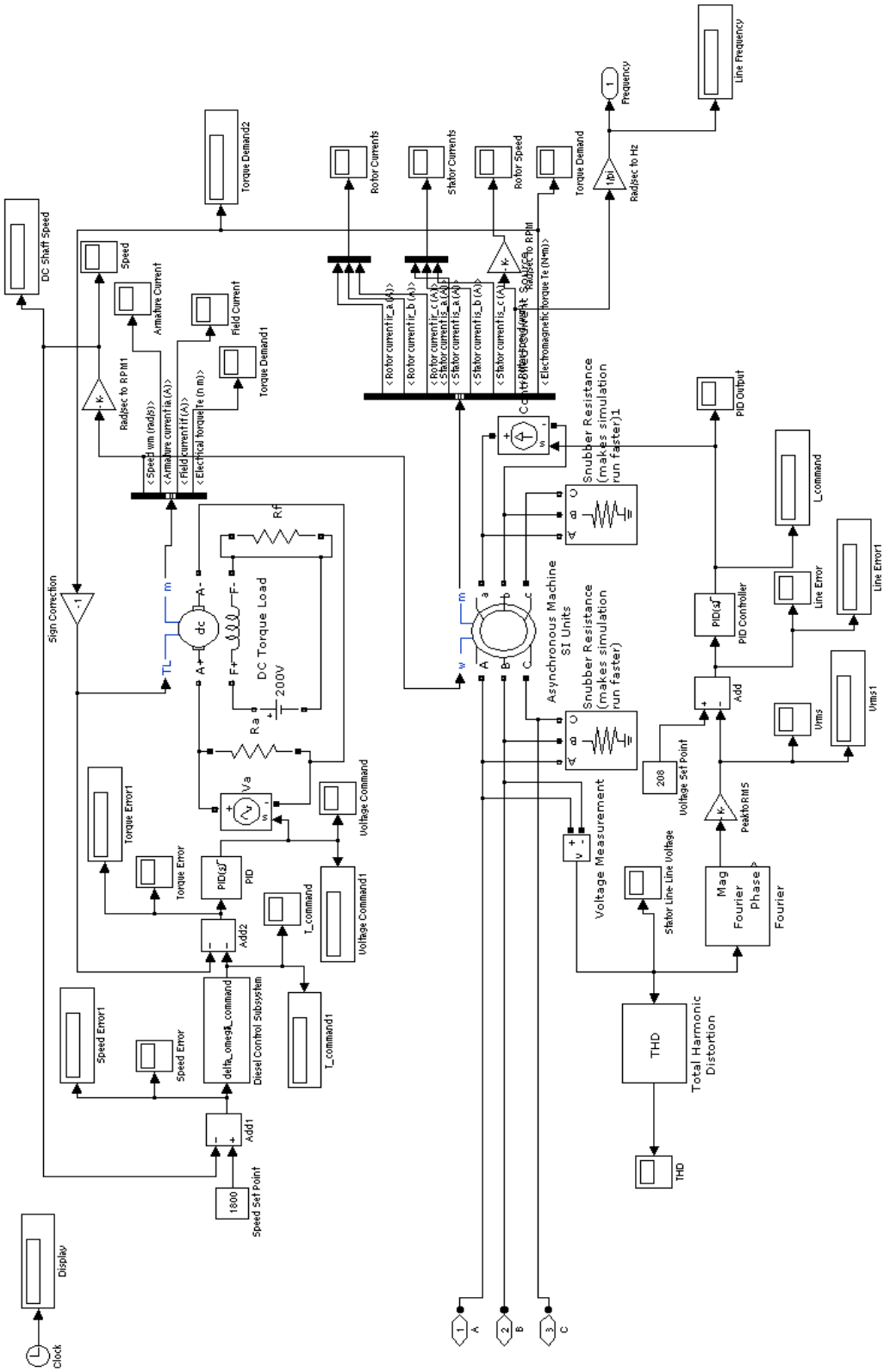

Figure 3-7 Diesel Generator Subsystem

The wound-rotor induction motor acts as the generator in this system. The stator connections of this machine are connected to the three phases of the microgrid bus through the diesel generator solid-state relay. There is a large resistive load in parallel with all three phases of the machine, which helps to prevent the singularities caused by connecting inductors to an ideal switch. The excitation system of this generator measures the phase A to phase B voltage on the stator and calculates the RMS value of this voltage by taking the magnitude of the Fourier transform of the signal at the fundamental frequency and dividing by $\sqrt{2}$. I initially found the RMS voltage using the SimPowerSystems RMS block, but this takes the RMS value over all frequencies, which can interfere with the convergence of the excitation system. Once the actual output voltage is measured, it is subtracted from a voltage set point of 208 volts before being fed into a PID controller that commands the current into the field windings of the wound-rotor induction machine. The parameters of this PID controller have a significant influence over the stability of the output voltage of the generator set, and small changes in these values can make the system unstable. Similar to the stator terminals, there is a large resistance in parallel with the rotor terminals that allows the matrix solver to converge. Also note that only two of the rotor windings are connected to a current source, but SimPowerSystems does not allow the third winding to remain completely disconnected.

4. Results and Conclusions

Using the model described in the previous sections, I was able to simulate several important aspects of the hardware system. In particular, I was able to simulate a short duration three-phase ungrounded fault on the microgrid bus while the diesel generator was operating at rated voltage and frequency with the induction motor load connected. The time duration for this particular simulation was 180 seconds. The first 20 seconds of the simulation allow for the diesel generator to come up to rated frequency and voltage before the induction motor is connected. Once the induction motor is connected at 20 seconds, the microgrid bus voltage is severely depressed while the induction motor comes up to rated speed. Once the induction motor reaches rated speed around 72 seconds into the simulation, the diesel generator is able to return the system to rated voltage. As can be seen in the plots below, the effect of the induction motor turn-on transient on system frequency is much less significant than its effect on system voltage. At 105 seconds, the system was in steady state operation with the induction motor load, and I induced a three-phase ungrounded fault on the system, the results of which can be seen below. After 30 cycles, or 0.5 seconds, I removed the fault from the system. For a fault this short in duration, the system was able to recover very quickly, returning to steady state voltage in less than a second.

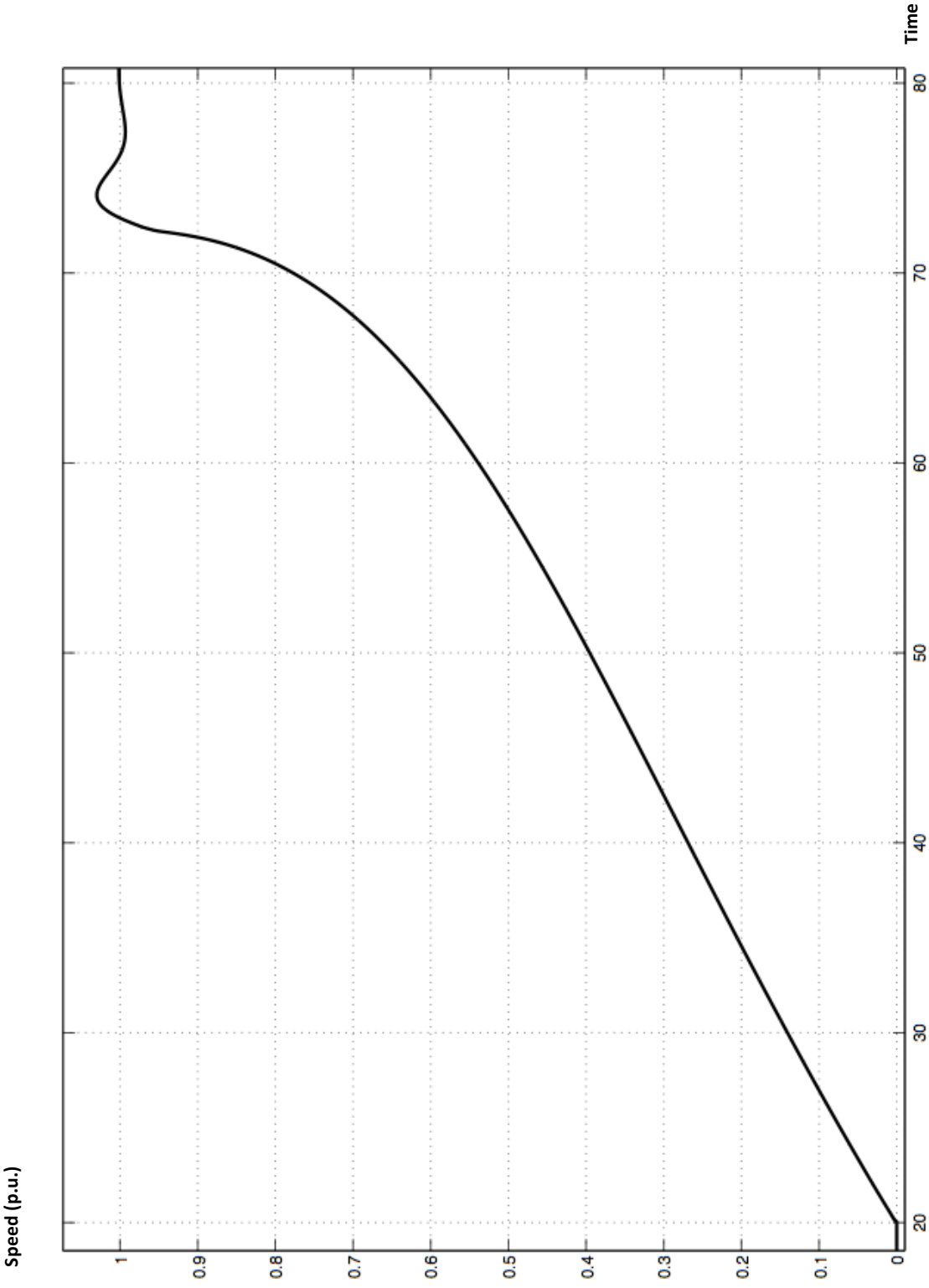

Figure 4-1 Induction Motor Starting Speed (per unit)

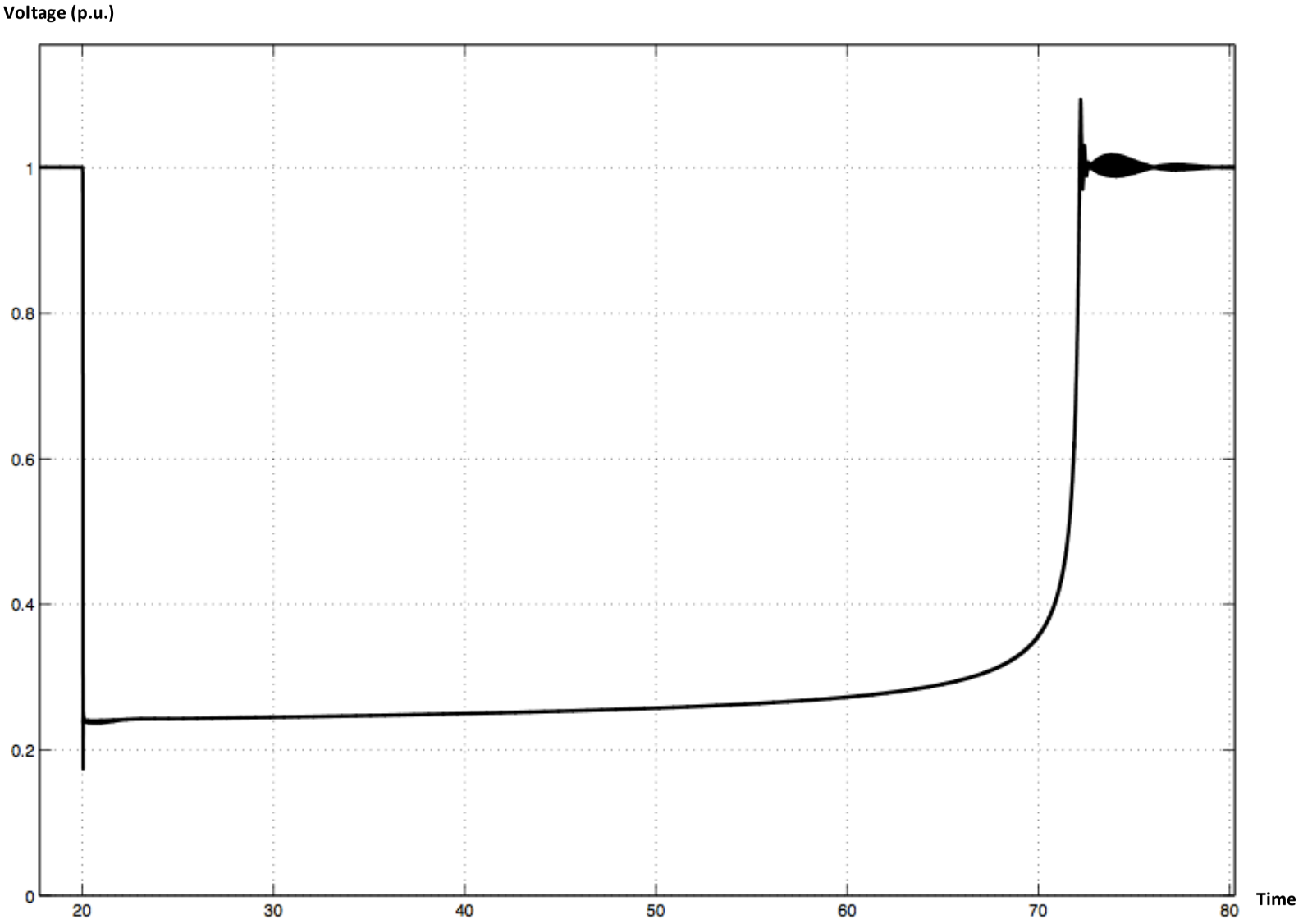

Figure 4-2 Microgrid Bus Voltage During Induction Motor Starting (per unit)

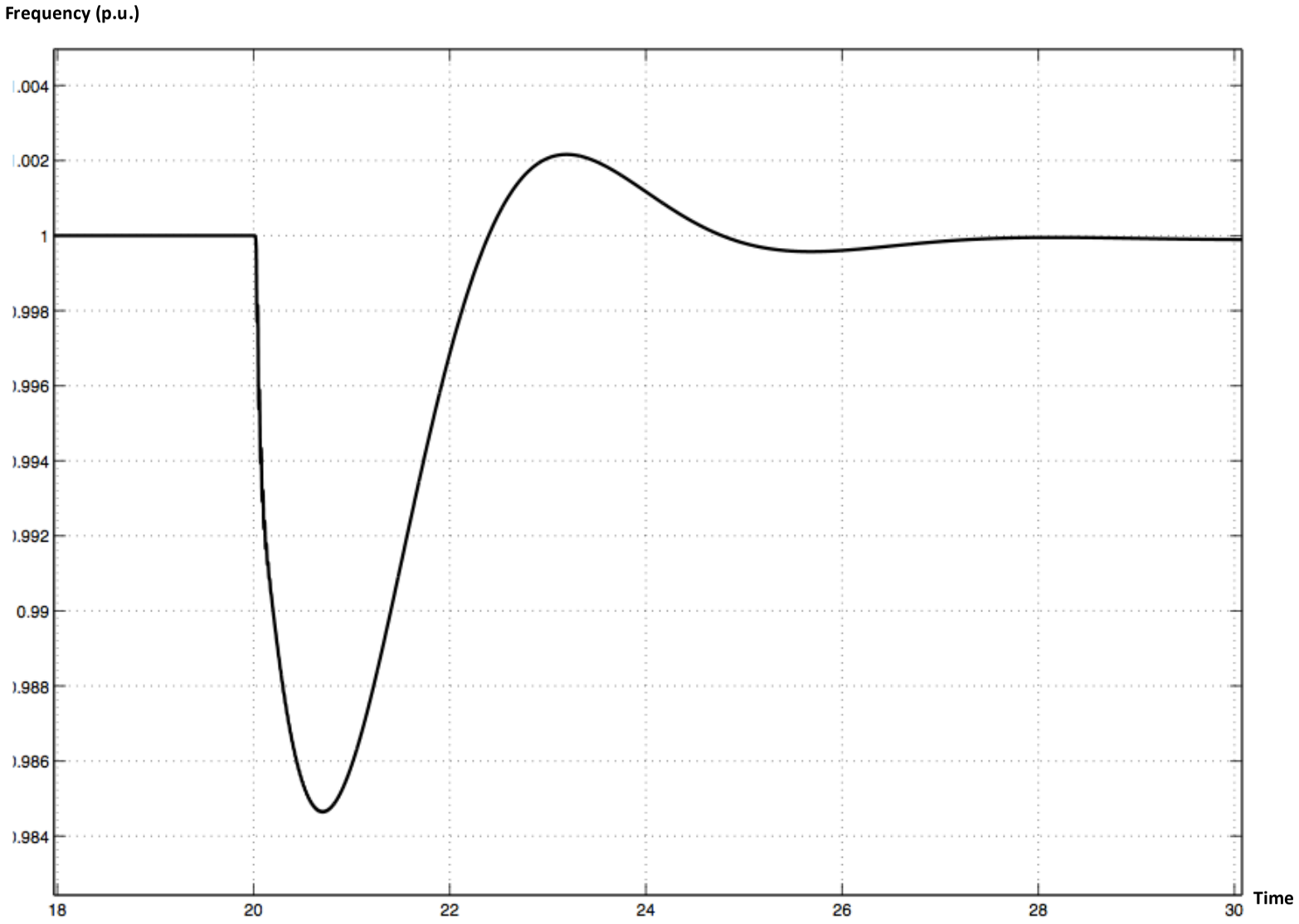

Figure 4-3 Microgrid Bus Frequency During Induction Motor Starting (per unit)

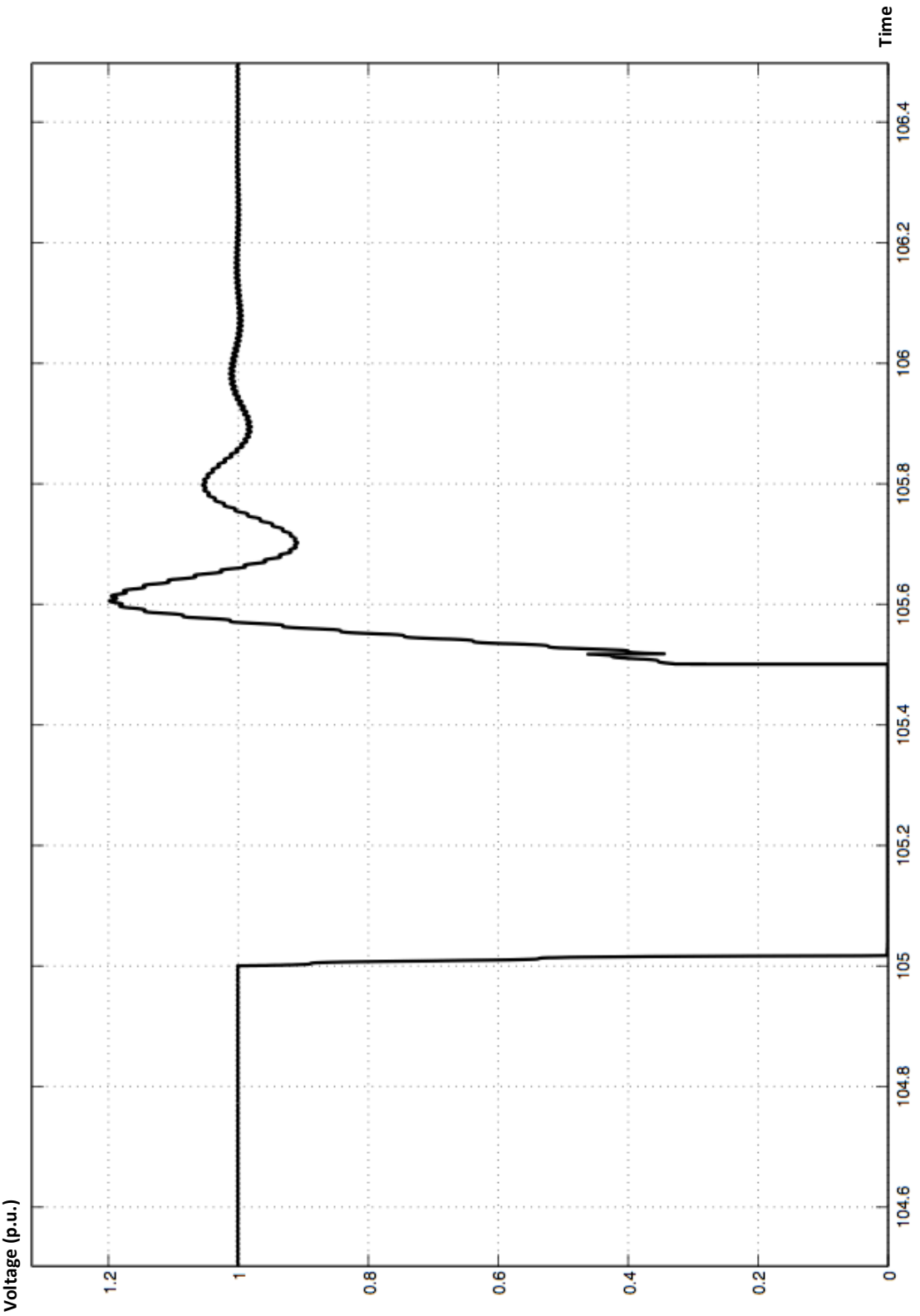

Figure 4-4 Microgrid Bus Voltage During Fault (per unit)

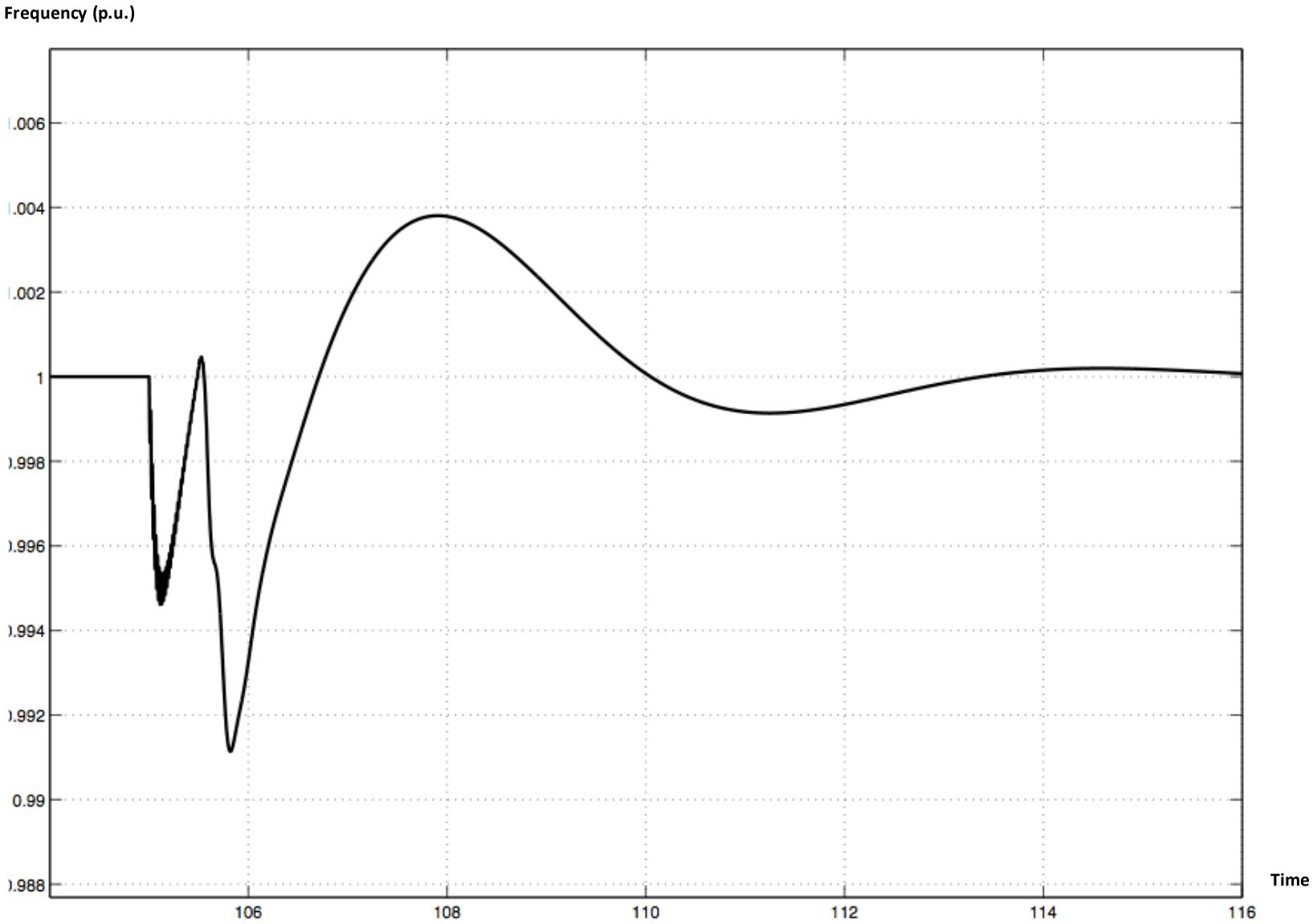

Figure 4-5 Microgrid Bus Frequency During Fault (per unit)

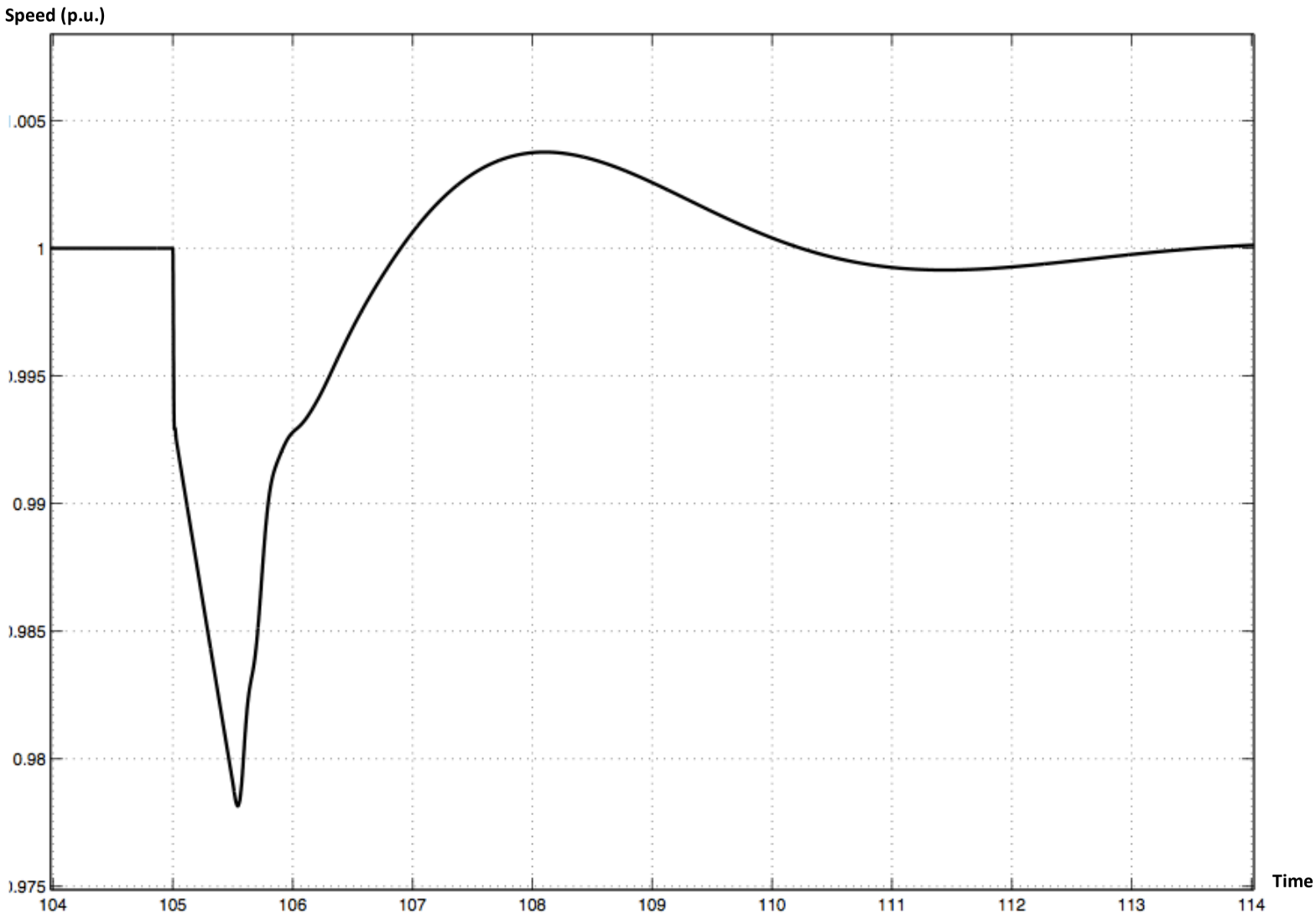

Figure 4-6 Induction Motor Speed During Fault (per unit)

In conclusion, using the Simulink model described above and the hardware system described in the attached document, it will be possible to design and execute experiments that will be able to investigate the performance of a microgrid under different conditions and configurations. In particular, with the completion of a few minor components in the hardware system, we will be able to induce an actual three-phase fault on our microgrid bus and investigate the response of the hardware system to fault-induced islanding. With a greater understanding of the impact of load type on fault-induced islanding and microgrid stability, it is our hope that microgrids will become a more common feature of the electric power grid.

Bibliography

Alaboudy, A. H. Kasem, H. H. Zeineldin, and J. Kirtley. "A Simple Control Strategy for Inverter Based DG to Enhance Microgrid Stability in the Presence of Induction Motor Loads." Masdar Institute.

Alaboudy, A.H. Kasem, H. H. Zeineldin, and J. Kirtley. "Impact of DG Interface Control, Microgrid Control Strategy and Load Type on Microgrid Stability." Masdar Institute.

Fitzgerald, A. E., Charles Kingsley, and Stephen D. Umans. *Electric Machinery.* 6th Edition. New York: McGraw-Hill, 2003.

IEEE Power Engineering Society. *Standard 112 - IEEE Standard Test Procedure for Polyphase Induction Motors and Generators.* The Institute of Electrical and Electronics Engineers, Inc., 2004.

IEEE Power Engineering Society. *Standard 113 - IEEE Guide: Test Procedures for Direct-Current Machines.* The Institute of Electrical and Electronics Engineers, Inc., 1985.

Lasseter, Bob. "Microgrids." U.S. Department of Energy Electricity Advisory Committee, 2011.

U.S. Department of Energy. "The Potential Benefits of Distributed Generation and the Rate-Related Issues That May Impede Its Expansion." 2007.

Appendix: Quick Reference Guide for Microgrid Simulink Model

This appendix is intended to serve as a quick reference guide for any user trying to run the microgrid Simulink model described previously in this document. Listed below are instructions for running the simulation and making changes to the system parameters. Each of the instructions below starts from the top interface of the Simulink model.

To change simulation parameters:

1. On the Simulink toolbar, click the Simulation menu, and in the list that drops down, click Configuration Parameters.
2. In the Solver tab, the start time and stop time of the simulation can be set. The solver type can also be set in this tab (ode23tb is recommended), as well as the maximum step size, minimum step size, and other parameters of the solver.

To run the simulation:

1. On the Simulink toolbar, click the Simulation menu, and then click Start.
2. After compiling and initializing, the clock will begin to display the current simulation time. After this clock reaches the simulation stop time, the simulation is done running. To view plots, double-click on the desired plotting block. To scale the axes automatically, click on the icon that looks like a pair of black binoculars. To zoom in to a specific region of the plot, click and drag on the plot to set the zoom area.

To change Diesel Generator Subsystem parameters:

To change induction motor parameters:

1. Double-click on the Diesel Generator Subsystem block.
2. In the subsystem window that appears, double-click on the Asynchronous Machine block.
3. In the Block Parameters window, on the Configuration tab, the most basic parameters can be set, including rotor type and preset model parameters. Do not change Mechanical Input, as this will decouple the shafts of the motor set. On the Parameters tab, all of the values of the equivalent circuit elements can be set. The values of the mechanical elements of this motor set are established in the DC motor model.

To change DC motor parameters:

1. Double-click on the Diesel Generator Subsystem block.
2. In the subsystem window that appears, double-click on the DC Motor block.
3. In the Block Parameters window, on the Configuration tab, the most basic parameters can be set, including the field type and preset model parameters. Do not change Mechanical Input, as this will decouple the shafts of the motor set. On the Parameters tab, the values of the equivalent circuit elements and mechanical model elements can be set.

To change DC motor PID controller gains:

1. Double-click on the Diesel Generator Subsystem block.

2. In the subsystem window that appears, double-click on the PID block closest to the DC motor block.
3. On the Main tab of the Block Parameters window, the gains of the PID controller can be set. On the PID Advanced tab, saturation limits and anti-windup methods can be specified.

To change excitation system PID controller gains:

1. Double-click on the Diesel Generator Subsystem block.
2. In the subsystem window that appears, double-click on the PID Controller block closest to the asynchronous machine.
3. On the Main tab of the Block Parameters window, the gains of the PID controller can be set. On the PID Advanced tab, saturation limits and anti-windup methods can be specified.

To change speed set point:

1. Double-click on the Diesel Generator Subsystem block.
2. Double-click on the Speed Set Point block, and in the Block Parameters window, change the Constant Value box to set the speed set point.

To change voltage set point:

1. Double-click on the Diesel Generator Subsystem block.
2. Double-click on the Voltage Set Point block, and in the Block Parameters window, change the Constant Value box to set the voltage set point.

To change Induction Motor Load parameters:

To change induction motor parameters:

4. Double-click on the Induction Motor Load block.
5. In the subsystem window that appears, double-click on the Squirrel-Cage Induction Motor block.
6. In the Block Parameters window, on the Configuration tab, the most basic parameters can be set, including rotor type and preset model parameters. Do not change Mechanical Input, as this will decouple the shafts of the motor set. On the Parameters tab, all of the values of the equivalent circuit elements and mechanical model elements can be set.

To change DC motor parameters:

4. Double-click on the Induction Motor Load block.
5. In the subsystem window that appears, double-click on the DC Motor Torque Load block.
6. In the Block Parameters window, on the Configuration tab, the most basic parameters can be set, including the field type and preset model parameters. Do not change Mechanical Input, as this will decouple the shafts of the motor set. On the Parameters tab, the values of the equivalent circuit elements can be set. The values of the mechanical elements of this motor set are established in the induction motor model.

To change load on the induction motor:

1. Double-click on the Induction Motor Load block.
2. In the subsystem window that appears, the load can be changed by changing the field voltage of the DC motor or the armature resistor on the DC motor. To change the field voltage, double-click on the Field Voltage Set Point block, and in the Block Parameters window, change the constant value to set the voltage value. To change the size of the armature resistor, double-click on the Armature Resistor block, and in the Block Parameters window, change the value in the Resistance block.

To change Phase-Controlled Load parameters:

To change the voltage cutoff percentage:

1. Double-click on the Phase-Controlled Load block.
2. In the subsystem window that appears, double-click on the Switch Controller block.
3. In the next subsystem window that appears double-click on the Monostable block.
4. In the Block Parameters window, change the cutoff percentage by modifying the Pulse Duration box. A cutoff percentage of 0% should be (100/100)*(1/120). A cutoff percentage of 100% should be (0/100)*(1/120), and other cutoff percentages are set linearly within these bounds.

To change the load parameters:

1. Double-click on the Phase-Controlled Load block.
2. In the subsystem window that appears, double-click on the 3 x 60W Lightbulb Array block.
3. In the Block Parameters window, change the configuration by selecting the appropriate option in the drop-down menu. Change the load characteristics by changing the values in the boxes.

To change passive load parameters:

1. Double-click on the passive load block, e.g., Resistor Bank 1, Inductor Bank, etc.
2. In the Block Parameters window, change the configuration by selecting the appropriate option in the drop-down menu. Change the load characteristics by changing the values in the boxes.

To change faulting parameters:

1. Double-click on the desired fault block: Microgrid Fault for a fault on the microgrid bus or Utility Fault for a fault on the utility bus.
2. In the Block Parameters window, change the type of fault (line-line, line-ground, etc.) by checking the top five boxes. The fault resistance can also be changed, as well as the ground resistance if a ground fault is selected and applied. Change the time that the fault occurs by changing the Transition Status and Transition

Times vectors. These vectors must be the same length. In Transition Status, “1” corresponds to a fault, and “0” corresponds to no fault.

To change switch parameters:

To change connection status of passive loads and Phase-Controlled Load:

1. Double-click the Load Switch Controller and Multimeter block.
2. In the subsystem that appears, double-click the manual switch to change the correspondingly numbered switch. A switch connected to “0” is open, and a switch connected to “1” is closed.

To change connection status of all other switches:

1. Double-click on the desired switch block, e.g., Main Microgrid SSR, Switch 6, etc.
2. In the Block Parameters window, set the initial status of the switch by selecting the appropriate option in the drop-down menu. Switching times are set in the Transition Times vector. Values in this vector set the time that the switch changes from the previous state, beginning with the initial status specified above. If no change is desired, do not set the Transition Times vector to an empty set, as this will trigger a transition in the first time step of the simulation; instead, enter a single value much higher than the run time of the simulation.

Reference Manual for Microgrid Hardware Simulation System

by

Jared P. Monnin

S.B., E.E. M.I.T., 2011

and

Michael M. Zieve

S.B., E.E. M.I.T., 2011

May 21, 2012

Table of Contents

List of Figures

1. Purpose

The purpose of this document is to act as a reference manual for the microgrid hardware simulation system currently being constructed in the Laboratory of Electromagnetic and Electronic Systems at the Massachusetts Institute of Technology, under the supervision of Prof. James L. Kirtley, Jr. In the following pages, we seek to explain in detail all of the work that has been accomplished on this project, from January of 2011 to the time of writing, in May of 2012. We have included detailed written descriptions, photographs, circuit diagrams, part numbers, links to datasheets, and in several cases, our rationale behind certain design decisions. We divided this report into sections based on the major components of the overall system, and we aim for each section to be largely independent of the other sections. It is our hope that anyone who joins this project in the future will be able to reference this document to answer any question they might have about the system we have put in place, as it existed at the time of writing.

2. System Overview

This section is a broad overview of the electrical and mechanical aspects of the project, describing the various components of the project, their interconnections, and their place within the wider project. Each component described in this section is described in detail later in this document.

2.1 Electrical Connections

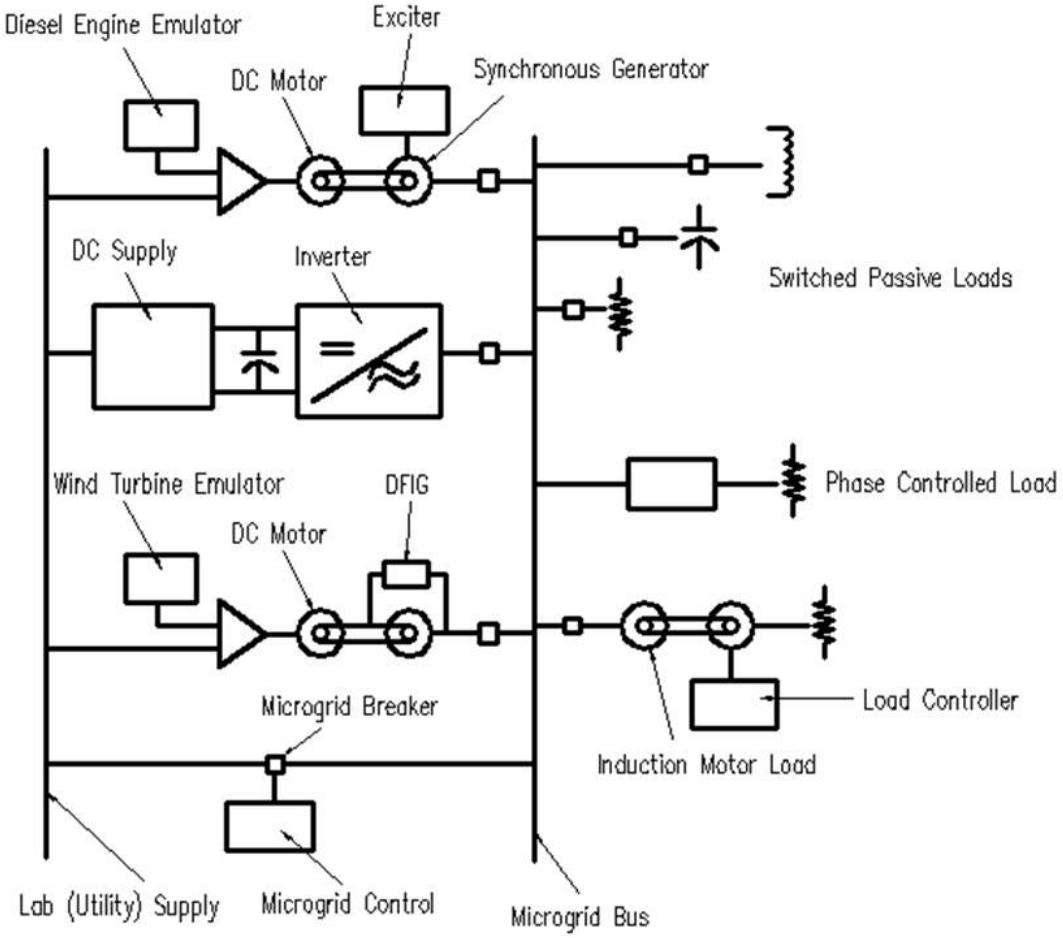

Figure 2-1 System Overview

The image above is a one-line diagram of the initial design of our project. At the time of writing, we have already implemented the microgrid bus, load and generator relays, resistive, capacitive, inductive, phase-controlled resistive, and induction motor loads, the solar farm emulator using the DC supply and inverters, the diesel generator emulation system, and a voltage and current measurement system.

2.1.1 Utility Connection

Power is supplied to the project from the lab utility supply through a rubber-insulated, three-phase, five-wire cable that should be connected only to the $120V_{l\text{-}n}/208V_{l\text{-}l}$ three-phase receptacle labeled L2 22. This receptacle is connected to breaker 22 in Load Center L2 to the right of the bus side of the project board, on the wall opposite room 10-097. The other end of this cable is connected to an emergency shut-off switch mounted on the project board under the project load center. Besides providing the ability to quickly disconnect power from the project, this box also contains three 30-ampere, 250-volt, Bussmann fuses. The emergency shut-off switch is then connected to the project load center, which contains the circuit breakers

Figure 2-3 Load Center and Outlets

Figure 2-2 Emergency Shut-off Switch

that connect and disconnect different parts of the project. Besides a breaker connecting the utility to the microgrid bus switch, there are breakers connecting several single-phase and three-phase power outlets on the project board that are used for auxiliary power supplies and monitoring systems. The breaker diagram is included below:

Figure 2-4 Load Center Breaker Diagram

1	1-phase Outlet C	Not Connected	2
3	Not Connected	1-phase Outlets A & B	4
5	Not Connected	Not Connected	6
7	Not Connected	3-phase Outlets L1	8
9	Not Connected	3-phase Outlets L2	10
11	Not Connected	3-phase Outlets L3	12
13	Microgrid L1	No Breaker	14
15	Microgrid L2	No Breaker	16
17	Microgrid L3	No Breaker	18
19	No Breaker	No Breaker	20

As noted above, the bottom left breaker in the load center connects the utility supply to the main microgrid solid-state relay. The other side of this relay is connected to our microgrid bus, which is constructed from a line of interconnected terminal strips. All of our loads are connected to this bus through electromechanical relays, and all of our generation sources are connected to this bus through solid-state relays. More information on these individual components, their associated control systems, the measurement system, and the methods

used to synchronize the microgrid bus to the utility supply are detailed in their respective sections below.

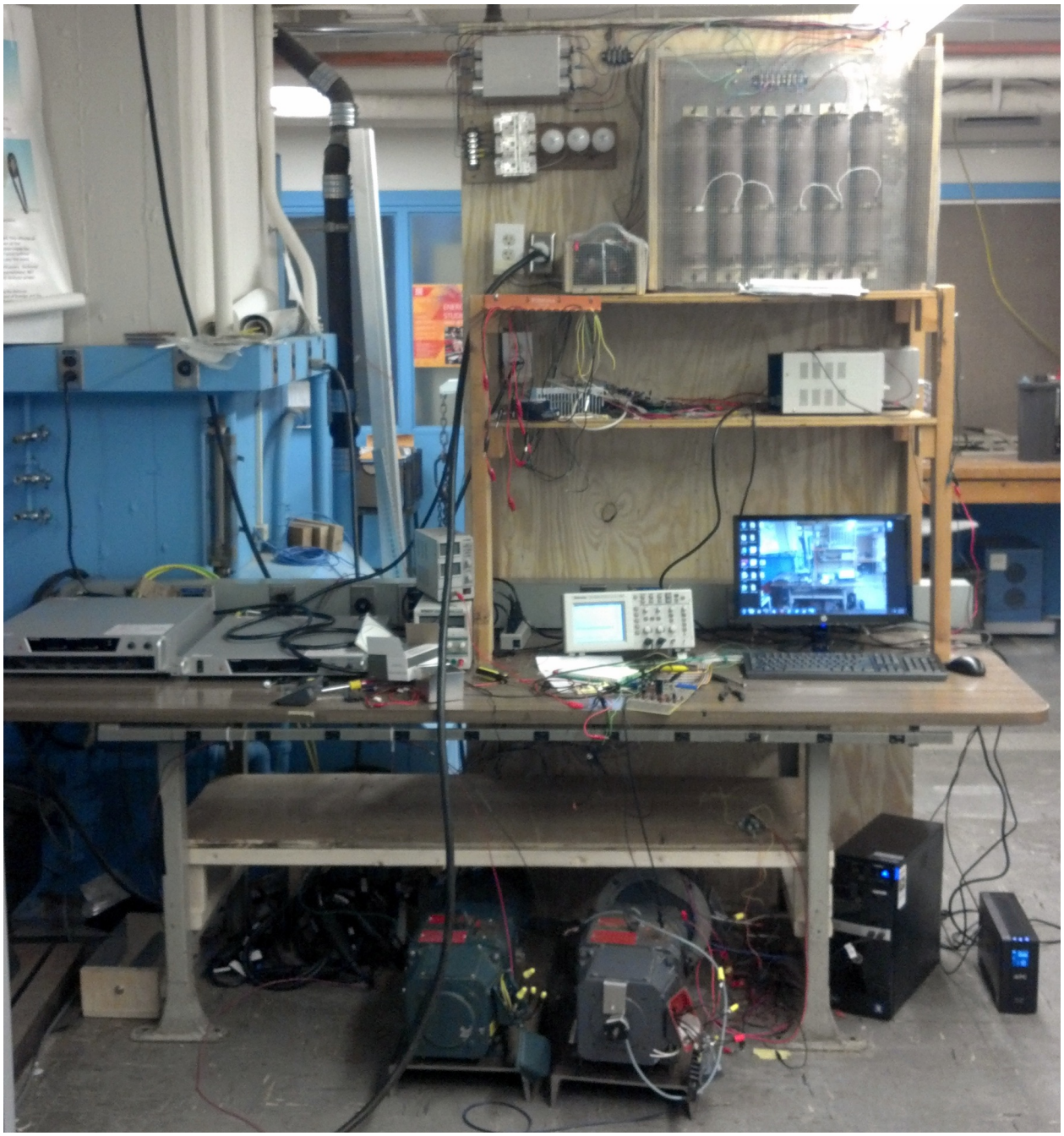

Figure 2-5 Load Side of Project Board

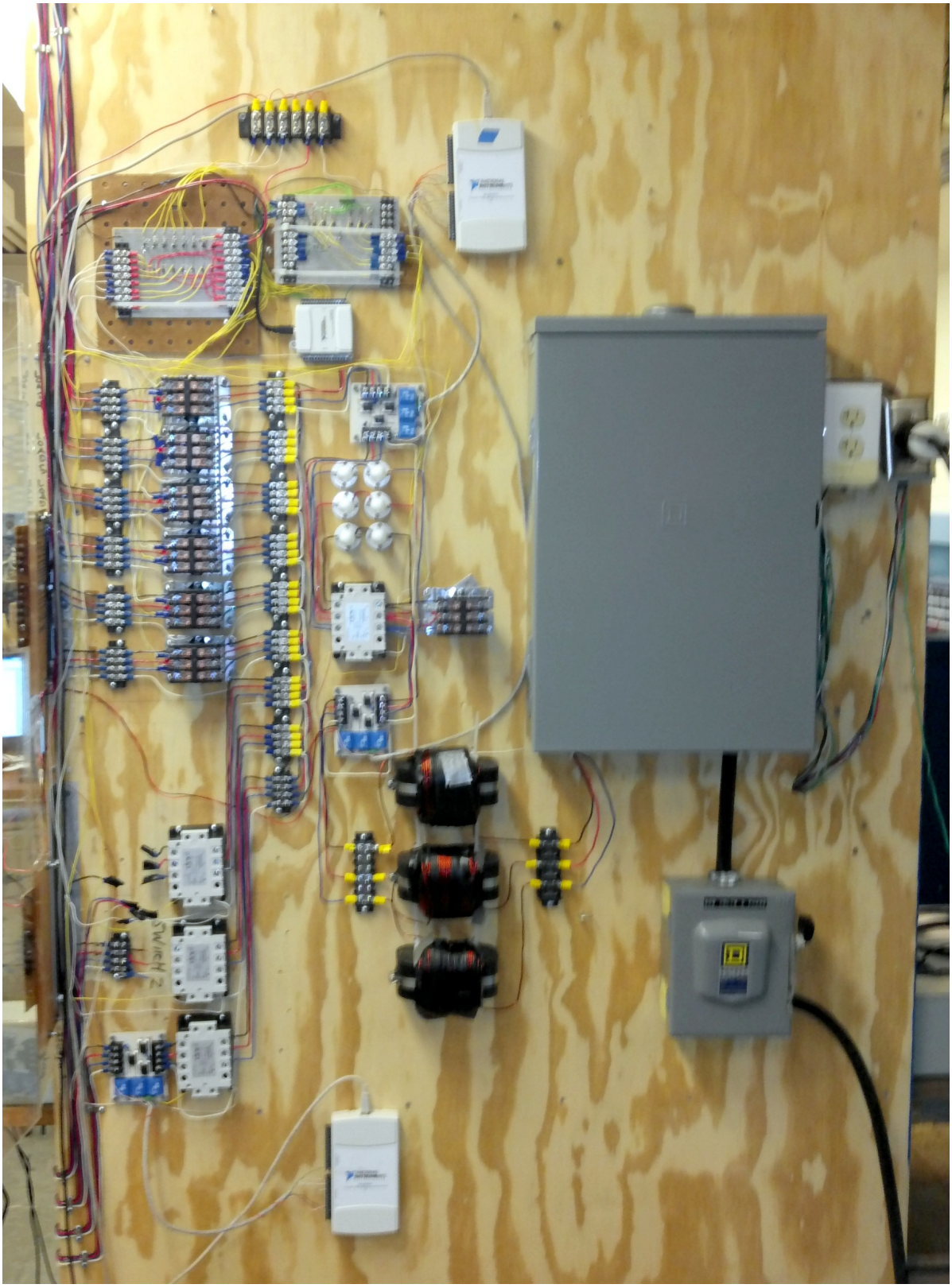

Figure 2-6 Bus Side of Project Board

2.1.2 Project Computer

Figure 2-7 Project Computer

Many of the components of our system described in later sections rely on our project computer, which is located under the desk on the load side of the project board. We purchased an HP desktop computer, the HP 505B Minitower Business PC with Windows 7, a monitor, and licenses for LabVIEW and other useful software. This computer interfaces with the measurement system DAQs and the Matsusada power supplies via several USB ports. Our main LabVIEW control interface runs on this computer, and all of the power supply control programs and dsPIC code versions can be found on this computer. As of the time of writing, the login information is:

Username: Programmer

Password: picogrid

We noticed that our computer was sensitive to the switching transients induced by our reactive loads, especially the induction motor load. During these transients, the computer would lose its connection to the control and measurement DAQs before quickly reconnecting to them, which interfered with data collection. This problem persisted even when we plugged the computer into a power outlet connected to a different load center, so we purchased an APC uninterruptible power supply and voltage regulator, which largely solved the transient problem.

2.1.3 Starting Procedure

The following checklist describes the steps in which the microgrid system should be started to ensure safe operation:

1. Turn on the computer and connect the DAQs via USB. With the DAQs powered up, launch LabVIEW, and run the control program.
2. Only after the DAQs are powered up and the LabVIEW program is running, turn on the power supply to the switches. **DO NOT TURN ON THE POWER SUPPLY WITHOUT LABVIEW RUNNING AND THE DAQS POWERED UP.** Turning on the power supply in this condition will turn on every switch on the board, with potentially catastrophic results.
3. Test each switch by clicking on the corresponding button in LabVIEW. The electromechanical switches will make an audible click. All switches have an LED indicator that turns on when voltage is applied to the switch.
4. Check the load center to ensure that the breakers are on or off as desired.
5. Connect the project to the utility power supply by plugging the main cable into the 3-phase outlet (L2 22) next to the project.
6. Turn the emergency off switch to the on position to power up the load center. At this point, if the bottom left breaker is on, the utility is connected to the main bus relay.
7. If generation sources are running and connected to the microgrid bus, **see the synchronization section before connecting the utility to the microgrid bus.** Failure to do so can result in large currents and torques on the motors, with potentially disastrous results.
8. Loads can now be connected and disconnected through the LabVIEW interface.

2.2 Hardware Mounting

As shown in Figure 2-5 and Figure 2-6 above, the emergency shut-off switch, load center, microgrid bus, and electromechanical and solid-state relays are all mounted on a vertical plywood board which is fastened to the back of a heavy workbench. We refer to this side of the project board as the “bus side”. On the workbench side of the project board, which we call the “load side”, we have constructed several shelves above and below the workbench. These shelves support several of our loads, some auxiliary power supplies, and important spare parts for the system. The shelf beneath the desk is intended to hold all of the control boards and power supplies for the motor sets used in the diesel generator, wind farm emulator, and induction motor load systems.

2.3 Safety Measures

To prevent accidental contact with the electrical terminals on the bus side of the project board, we have constructed a clear fiberglass cover that latches to the load center with a weak permanent magnet and can be held shut more securely with a hook and rubber band connected to the cover. This cover should be latched securely before any power is connected to any part of the microgrid system. On the load side of the project board, we have constructed wood and metal screening covers for all accessible components that might present an electrical or thermal hazard if accidentally touched. In the event of any unintended fault on the system or any electrical accident, power to the microgrid should immediately be disconnected by shutting off the emergency shut-off switch. Utility power and all microgrid generation sources and loads can be isolated from the microgrid bus by shutting off the switch driver board power supply.

3. Generators

There are currently two generation sources in our system, with the possibility of adding a third source in the near future. These generation sources are described in this section.

3.1 Diesel Generator

The diesel generator is the master generator in the microgrid because it sets the voltage, phase and frequency of the system in the absence of the utility. The diesel generator is designed to supply between 500 watts and 1 kilowatt of power to the microgrid. The diesel generator in our system is comprised of a 1.5-horsepower DC motor and a 1.0-horsepower wound-rotor induction motor. The two motor shafts are coupled together using a 22-mm Lovejoy Sintered Iron Jaw Coupling with a LOVEJOY Buna-N Insert (size A/L075) and are mounted together on a steel plate. Note for future applications, the actual shaft size is a standard 7/8-inch shaft and the metric 22-mm shaft coupling was bored out another 0.023 inches in order for it to fit properly on the shaft.

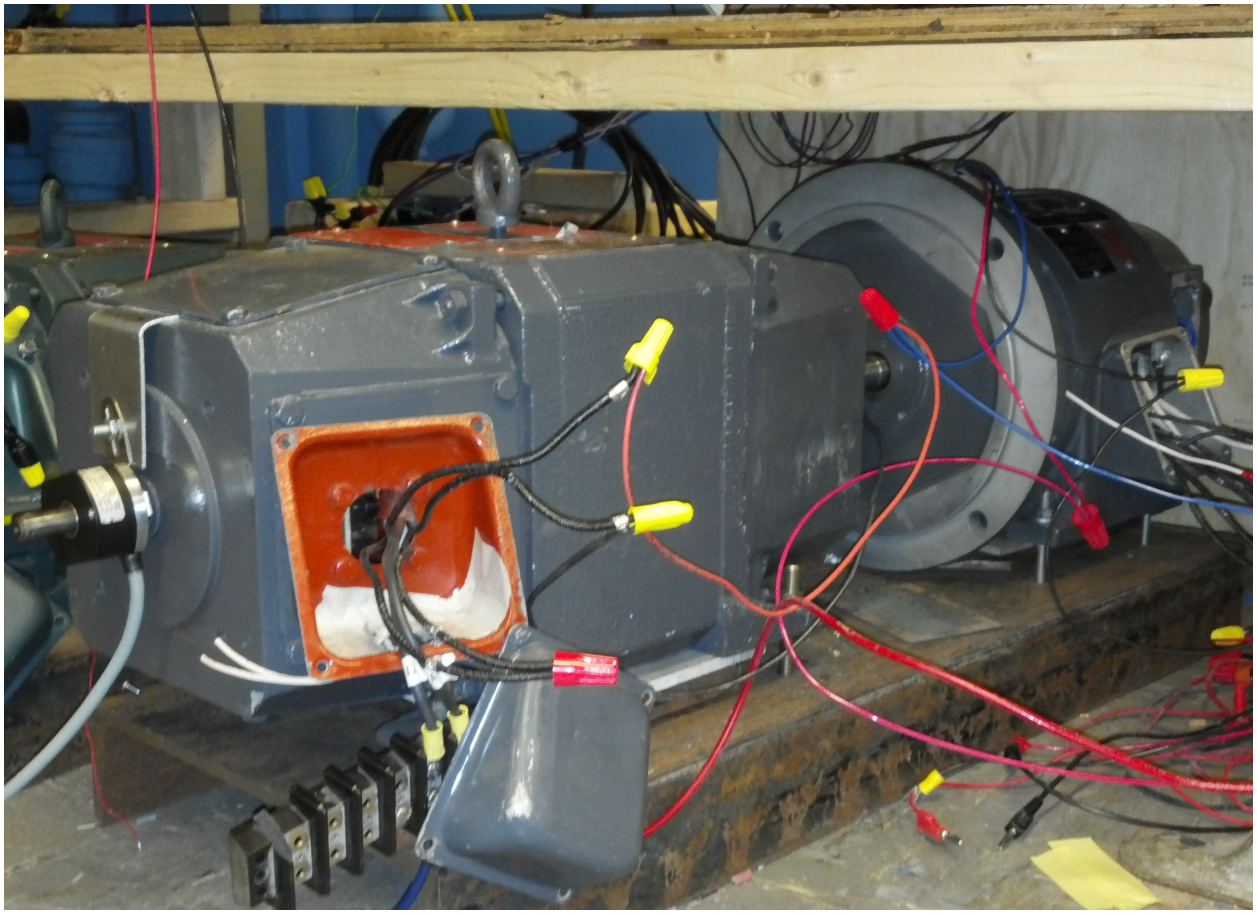

Figure 3-1 Diesel Generator (DC Motor on left and Induction Motor on right)

3.1.1 Accessories

Figure 3-2 Red Lion ZPJ

Mounted on the secondary shaft of the DC motor is a Red Lion ZPJ large through-bore rotary pulse generator. This incremental encoder has three NPN Open Collector Transistor outputs that provide standard A, B and Z encoder quadrature outputs. Output B leads output A by 90 degrees for counter-clockwise rotation of the motor shaft and each of these outputs provides 2500 pulses per revolution. The Z output provides an index pulse and therefore outputs one pulse per revolution. There are 2500*2 + 1 = 5001 pulses per revolution, which provide a high resolution measurement for the direction, speed and position of the rotor. Note

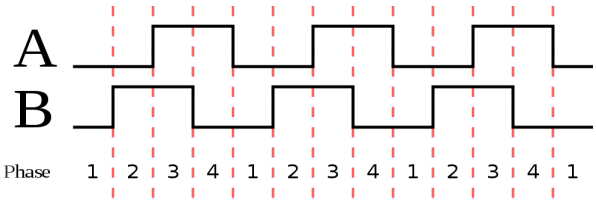

Figure 3-4 Counter-Clockwise Quadrature Encoder Logic

that while position can be calculated, only the direction and speed of the rotor shaft are used. It is important that all of these outputs are connected to the desired output voltage, in our case +5VDC, through pull-up resistors or else there will be no output. Additionally, the encoder is mounted to the secondary shaft side of the DC Motor such that it is centered on the secondary shaft. To ensure a firm connection between the internal coupling of the encoder and the DC motor secondary shaft, a 12-mm insert is used. Note for future use, the secondary shaft is actually 0.5 inches, or 12.7 mm.

There is also an Allegro Microsystems Inc. ACS712 current sensor board, which we used to measure the current driving the DC motor. The 05B version of the board has a current measuring range for both alternating and direct current within the range of ±5.0 amperes. A zero ampere measurement results in a nominal 2.5-V output with a 185-millivolt per ampere sensitivity in measurement. For example, if one ampere is flowing in the positive direction through the current sensor, it will output 2.5 + 0.185 = 2.685 volts. Note that we use a few varieties of Allegro Microsystems current sensor boards, all with different current ranges and sensitivities. The 05B model is used in the diesel generator system because it provides the highest resolution in the desired current range.

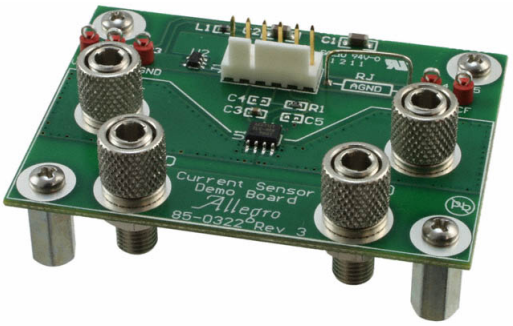

Figure 3-3 ACS712 Current Sensor Board

Additionally, there is a dsPICDEM MC1 Motor Control Development Board, which we use as the controller for the system. The board uses a Microchip dsPIC30F6010 High Performance Digital Controller as its central processor. The dsPIC30F6010 has a 16-bit architecture and has 80 pins, 68 of which have I/O functionality. It also has functionality for 8 pulse width modulation channels. The dcPIC30F6010 can be removed and replaced by another microcontroller if needed simply by replacing the mounted red card, as shown below.

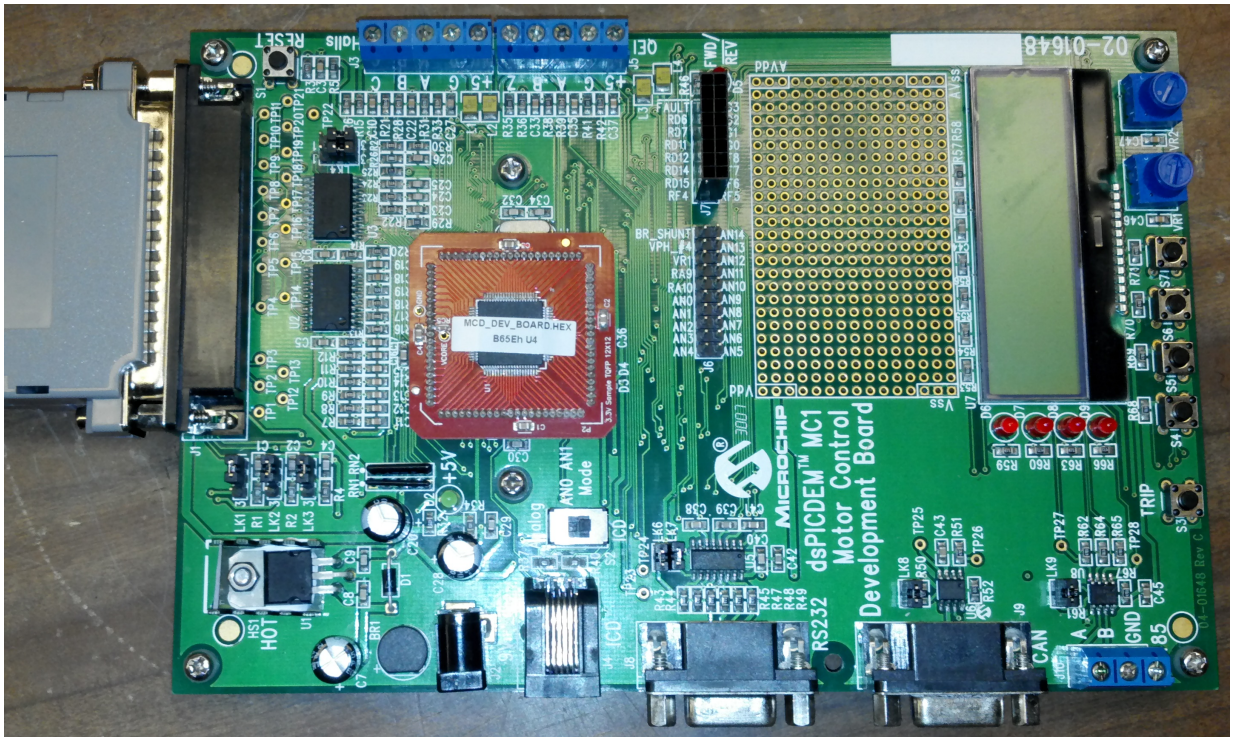

Figure 3-5 MC1 Motor Control Development Board

The Motor Control board and dsPIC are programmed using the free MPLAB Integrated Development Environment software that can be downloaded from www.microchip.com. This software supports programming in both Assembly and C. To debug and program the dsPIC, the MPLAB ICD 3 In-Circuit Debugger 3 System is used. This system connects to the computer via USB and programs the dsPIC via an Ethernet cord connected to the ICD port on the board.

Note that to properly use the ICD 3, the AN0 Mode switch must be switched from its Analog position to ICD.

Figure 3-6 MPLAB ICD 3

3.1.2 Model

While the DC motor acts as the prime mover and the coupled induction motor acts as the three-phase generator, what makes this system emulate a diesel generator is our use of the diesel generator governor model shown below:

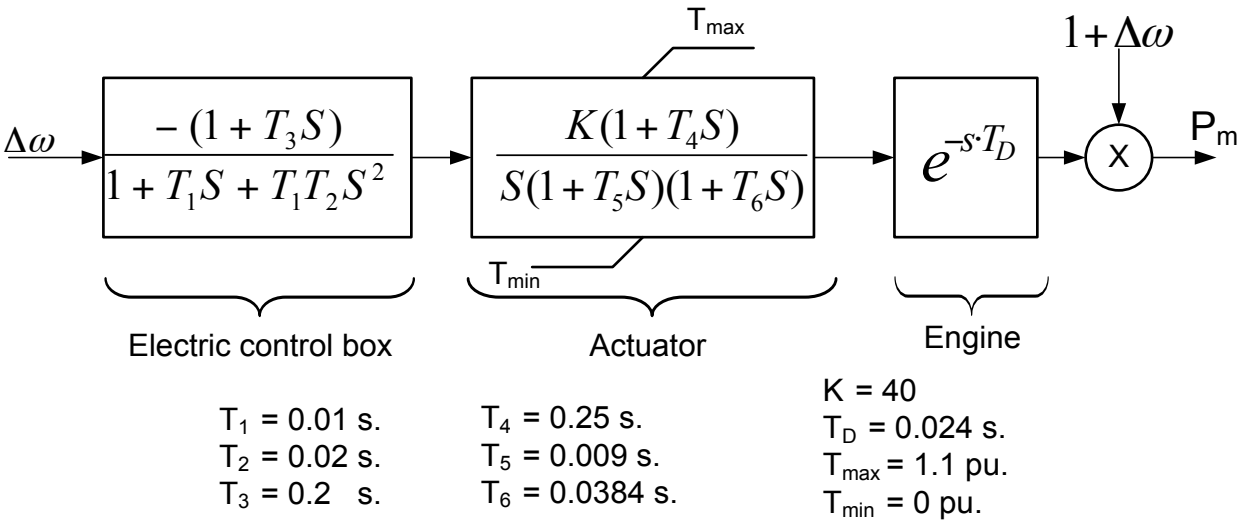

Figure 3-7 Diesel Generator Governor Model

The diesel generator governor model represents a continuous time transfer function that models the behavior of a diesel generator. It takes an input of a mechanical frequency error

and outputs a power command. Because torque multiplied by mechanical frequency is power, $P_m = T * \omega$, the torque output of the system is what is measured in our model. For a DC motor, torque is proportional to armature current, so we measure the current used to drive the DC motor and scale it such that it represents the torque output of the system. Similarly, we measure the rotational speed of the motor shaft using the encoder to determine the mechanical speed, which allows us to determine the frequency error. For simplicity, the diesel generator system that we implemented can be thought of as a simple block diagram:

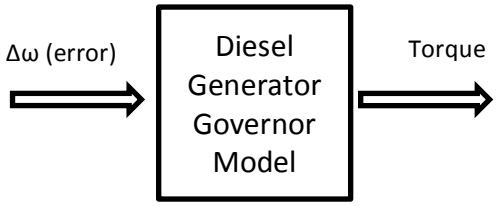

3.1.3 I/O

The diesel generator system combines many different parts and boards. Descriptions of the various pin-outs are listed below for each motor and component.

DC Motor

DC Motor Wires	Color	Connection
F1	Black	V+ (Field Power Supply)
F2	Black	F3 (on DC Motor)
F3	Black	F2 (on DC Motor)
F4	Black	V- (Field Power Supply)
A1	Black	IP- (on Current Sensor Board)
A2	Black	(Power) Ground
Temperature Sensor (2)	White	Not Connected

This DC motor field configuration results in a high voltage connection where the field windings are connected in series.

Synchronous Generator (Wound-Rotor Induction Motor)

Generator Wires	Color	Connection
T1	Black	T7 (Induction Motor)
T2	Black	T8 (Induction Motor)
T3	Black	T9 (Induction Motor)
T4	Black	T5 and T6 (Induction Motor)
T5	Black	T4 and T6 (Induction Motor)
T6	Black	T4 and T5 (Induction Motor)
T7	Black	T8* and T9* (Induction Motor)
T8	Black	T7* and T9* (Induction Motor)
T9	Black	T7* and T8* (Induction Motor)
M1	White	V+ (Synchronous Generator Supply)
M2	White	V- (Synchronous Generator Supply)
M3	White	Not Connected

Note that connections with a * such as T7-T8 -T9 are all internally connected.

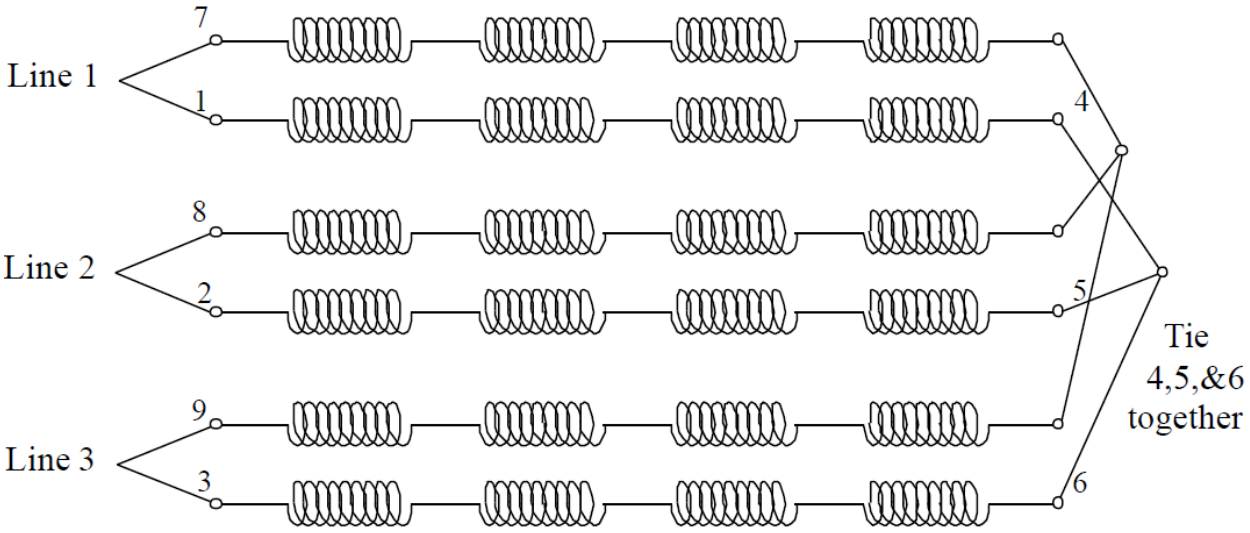

Figure 3-8 Synchronous Generator Armature Windings

This configuration of the armature windings allows for a three-phase AC output.

Encoder

Encoder Wires	Color	Connection	I/0	A/D
+VDC	Red	+5V on QEI connector (on Motor Control Board)	Input	Power
COM	Black	G on QEI connector (on Motor Control Board)	Input	Ground
A	White	A* on QEI connector (on Motor Control Board)	Input	Digital
B	Green	B* on QEI connector (on Motor Control Board)	Input	Digital
Z	Orange	Z* on QEI connector (on Motor Control Board)	Input	Digital

Note that connections with a * such as A, B and Z are all additionally connected through a 1000-ohm pull-up resistor to +5VDC.

Current Sensor Board

Current Sensor Board Pins	Color	Connection	I/O	Type
Vin	N/A	Not Connected	NC	NC
+5V	N/A	+5V (on Motor Control Board)	Input	Power
AGND	N/A	Ground (on Motor Control Board)	Input	Ground
Vout	N/A	AN2 (on Motor Control Board)	Output	Analog
CF	N/A	Not Connected	NC	NC
IP+	N/A	Motor Output 1 (from Inverter1)	Input	Analog
IP-	N/A	A1 (on DC Motor)	Output	Analog

Note that to connect to the Current Sensor Board, a 6 position WM4267-ND Connection Housing is needed for the board, and the incoming wires must be crimped with a WM2510-ND Female Connection Terminal.

dsPIC Board (dsPICDEM MC1 Motor Control Development Board)

The dsPIC board is powered by a +9VDC wall adaptor that plugs into the 9N IN connector. As mentioned earlier, the ICD3 Ethernet cord connects to the ICD port for debugging and programming, and the ANO switch must be switched to ICD for it to work. The dsPIC board has many different signal connection points, and therefore the listing is broken up by connection terminal.

dsPIC Board (J1 connector)	**Wire Color**	**Connection**	**Test Point**	**I/O**	**Type**
Pin 13 (PWM Phase 1 HIGH)	Yellow	Inverter input 1	TP18	Output	Digital
Pin 31 (PWM Phase 1 LOW)	Green	Inverter input 2	TP8	Output	Digital
Pin 12 (PWM Phase 2 HIGH)		Inverter2 input 1	TP17	Output	Digital
Pin 30 (PWM Phase 2 LOW)		Inverter2 input 2	TP7	Output	Digital
Pin 19 (+5V)			N/A	Output	Power
Pin 18 (Ground)			N/A	Output	Ground

Note that the J1 connecter is a Male D-subminiature 37 (37 pins).

dsPIC Board (QEI port)	**Color**	**Connection**	**I/O**	**Type**
+5	Red	+5V on Encoder	Output	Power
G	Black	COM on Encoder	Output	Ground
A	White	A on Encoder	Input	Digital
B	Green	B on Encoder	Input	Digital
Z	Orange	Z on Encoder	Input	Digital

dsPIC Board (J7 port)	**Color**	**Connection**	**I/O**	**Type**
AN2	Yellow	Vout (on Current Sensor Board)	Input	Analog
VR1		AN0 (on dsPIC Board)	Output	Analog
AN0		VR1 (on dsPIC Board)	Input	Analog

Note that to connect to the J7 port, a 16-position WM2525 Connection Housing is needed for the board and the incoming wires must be crimped with a WM2510-ND Female Connection Terminal.

3.2 Solar Farm

The solar farm hardware simulation in our project is meant to emulate an array of photovoltaic modules that can provide three-phase power to a microgrid using small power inverters. We built a basic version of this hardware simulation using three microinverters and a USB-controllable DC power supply connected to the project computer.

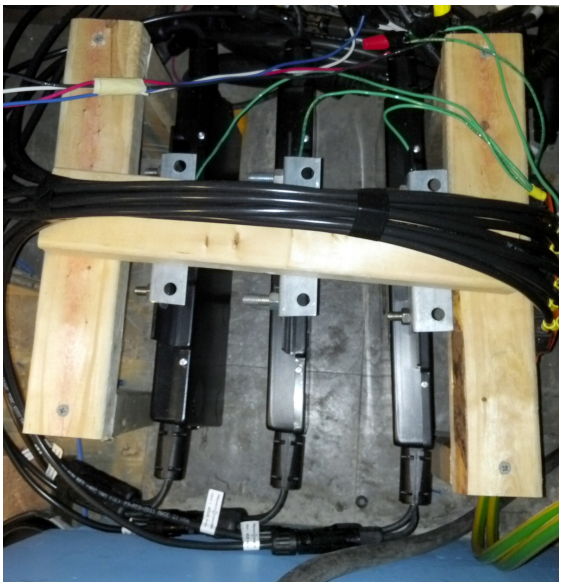

Figure 3-9 Enphase Microinverter Array

3.2.1 Inverter Array

Rather than build inverters from scratch, we purchased three Enphase D380 microinverters. These inverters are capable of outputting up to 380 watts each at $208V_{line\text{-}line}$ and can accept input voltages of 28V to 56V DC. These three inverters are mounted on a wooden frame, which sits to the left of the project board on the load side of the board. The microinverter input wires are terminated with MC4 connectors, so we bought six MC4 extension cables, cut them in half, and used them to connect the twelve microinverter inputs to a terminal strip, which we then connected to the V+ and V- wires of the DC power supply. Note that the Enphase D380 is actually a dual-pack module consisting of two Enphase M190 modules, so there are twice as many electrical connections as one might expect. Once we connected the module inputs to a terminal strip, we used an Enphase AC Branch Cable to connect the module outputs in a Y configuration with the neutral point connected to the neutral wire of our microgrid bus. This branch cable was then connected to the third solid-state relay (counting from the top of the board) on the bus side of the project board.

To start the inverters, the DC power supply should be connected and turned on first, outputting a voltage within the range of acceptable starting voltages. There are large capacitors in the microinverters, so there will be a large charging current for a few seconds when the DC power is first applied. Once the DC input has been applied for approximately one minute, the status LEDs will blink green six times, and the microinverters can be connected to the microgrid bus. Since the microinverters do not support voltage independently, no synchronization is necessary before closing this relay. Upon detecting rated voltage on the output, the microinverters have a 5-minute commissioning period before they will begin to output power. At the end of the commissioning period, the LED indicators should begin to blink orange, signifying that they are outputting power but are not synced up to an optional monitoring system (the Enphase Envoy) that we did not purchase. At this point, the DC power supply should be outputting full current if the voltage limit is set sufficiently high. If the microinverters are not outputting current at this point, but the voltage on the DC supply is experiencing transients, it will help to connect a resistive load and increase the current limit of the power supply. For troubleshooting issues, the LED indicators on the back of the modules will output troubleshooting codes that can be looked up in the datasheet (see appendix for datasheet link).

3.2.2 DC Power Supply

For the DC power supply in this system, we purchased a Matsusada RE45-45-LUs1 power supply, which is capable of outputting 45 amperes at 45 volts. This model also comes with a USB control module, which allows us to command voltage and current output using the project computer. This power supply currently sits on the left side of the lab table on the load

side of the project board. It is connected to the microinverter array under the table with 4-gauge (AWG) cables, which allow us to take full advantage of its 45-ampere output.

Figure 3-10 Matsusada DC Power Supply

We have written a basic C++ program that communicates with the power supply and can cycle through a vector of output voltages and currents, with an arbitrary time delay between samples. This program allows us to control the power supply to behave like a simple model of a photovoltaic module. Using data from the National Renewable Energy Laboratory's (NREL) Oahu Solar Measurement Grid (National Renewable Energy Laboratory 2011), we can command realistic outputs from the DC power supply with as little as one second of delay between samples. The data from NREL's dataset is a measurement of solar irradiance, but with the relations between solar irradiance and voltage and current approximated as

$$I_{out} \propto \Phi \qquad \text{and} \qquad V_{out} \propto \ln(\Phi),$$

where Φ is the solar irradiance, it is simple to derive current and voltage pairs that fluctuate as a function of the solar irradiance.

3.2.3 Future Work

One of the biggest flaws in the current solar farm system is the inability of the microinverters to independently support an output voltage. In other words, our solar farm can only operate in conjunction with another generation source. This is less of a problem if we always have the utility connected or the diesel generator running, but it limits the ways in

which the solar farm can contribute to the stability of the microgrid during transients. Future work could include replacing the current microinverter array with a set of inverters that can implement real and reactive power droop control or current injection control. This new system should be able to support voltage independently of the other generation sources and would potentially be able to greatly improve the stability of the microgrid during fault-induced islanding and other transients (Alaboudy, Zeineldin and Kirtley n.d.).

3.3 Wind Farm

At the time of writing, only the diesel generator and solar farm simulations have been developed to the point of operation; however, we have also made progress toward the development of a wind farm hardware simulation. The wind farm will emulate the electrical

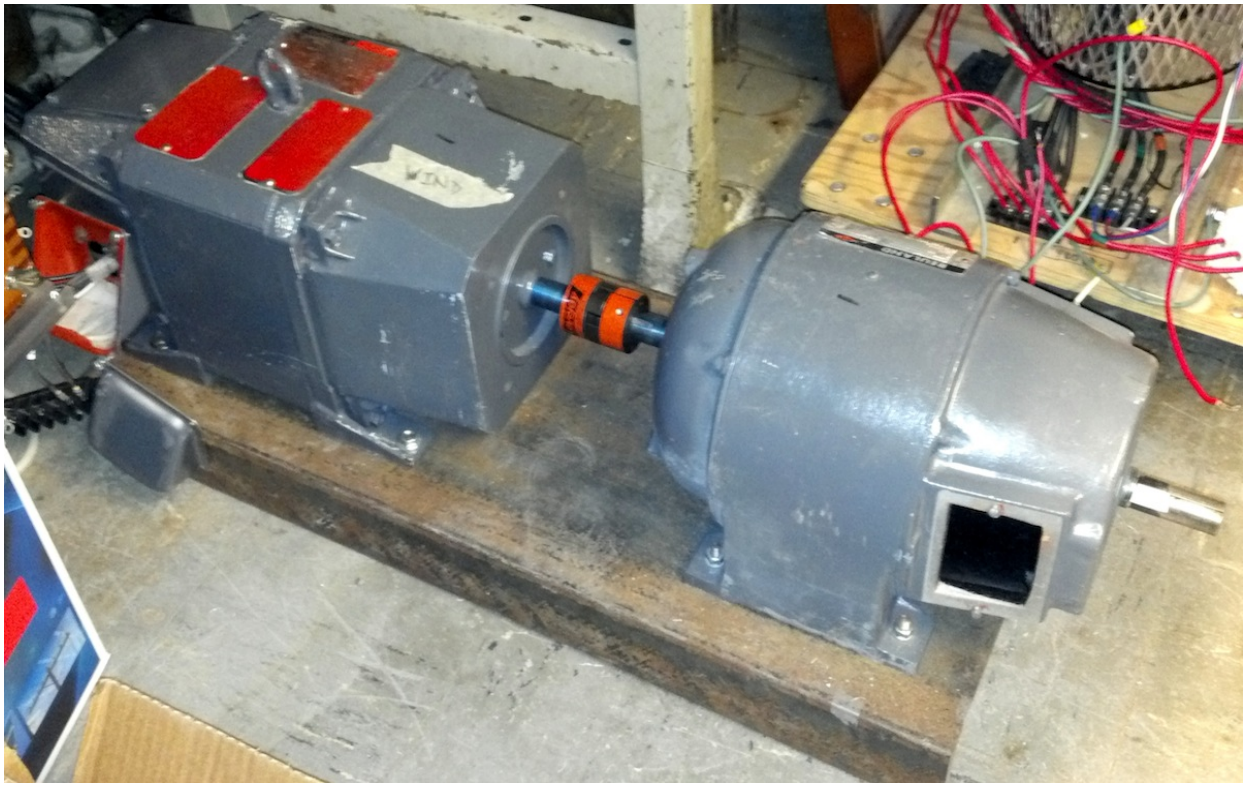

Figure 3-11 Wind Farm Motor Set (DC Motor on left, Induction Motor on right)

properties of a doubly fed induction generator driven by a wind turbine.

3.3.1 Hardware

The prime mover in this system, the wind turbine, will be modeled using a 1.5-horsepower DC motor identical to those motors used in the diesel generator described above and in the induction motor load described in the Loads section. This motor is mechanically coupled to a 1-horsepower wound rotor induction motor using the same Lovejoy jaw coupling described above, again with the 22-mm inner diameter bored out to fit the 7/8-inch shaft of the motors. The wound rotor induction motor will serve as the doubly fed induction generator thanks to the slip rings that provide access to the rotor windings. These two motors are mounted on a heavy steel base, and the motor set is currently stored under a desk in the corner of the project work area. Using the procedures outlined in IEEE Standard 112 and IEEE Standard 113, we found the parameters of the motors to be the following:

Table 1 - Wound Rotor Induction Motor and DC Motor Parameters

Induction Motor	
X_1	4.0Ω
X_2	4.0Ω
X_m	69.3Ω
R_c	469.7Ω

DC Motor	
Armature Resistance	0.7Ω
Armature Inductance	0.032H
Field Resistance	275Ω
Field Inductance	7.5H
Armature to Field Mutual Inductance	2.97H

3.3.2 Design and Future Work

To get the DC motor to emulate a wind turbine, we designed a simple buck converter circuit that would drive the armature of the DC motor at an arbitrary voltage. With a constant

voltage on the field of the DC motor, we can control the shaft speed by adjusting the duty cycle of the buck converter with a simple microchip. Using wind data from the National Renewable Energy Laboratory, it would be straightforward to derive a set of desired duty cycles, which can then be stored on the microchip and passed to the buck converter at arbitrary time delays. In this way, we could control the shaft speed of the DC motor to emulate the mechanical characteristics of a wind turbine. We have purchased the components to build this circuit, including the microchip, but it has not yet been built.

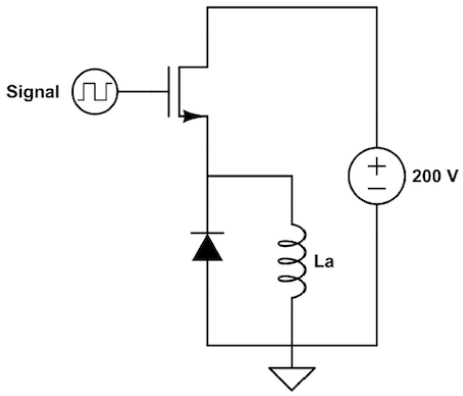

Figure 3-12 DC Motor Armature Buck Converter

On the generator side of the motor set, the present design calls for the construction of a back-to-back converter that can feed power to the rotor of the wound rotor induction generator when it is running below synchronous speed and can feed power from the rotor to the grid when it is running above synchronous speed. Controlling all twelve of these transistors

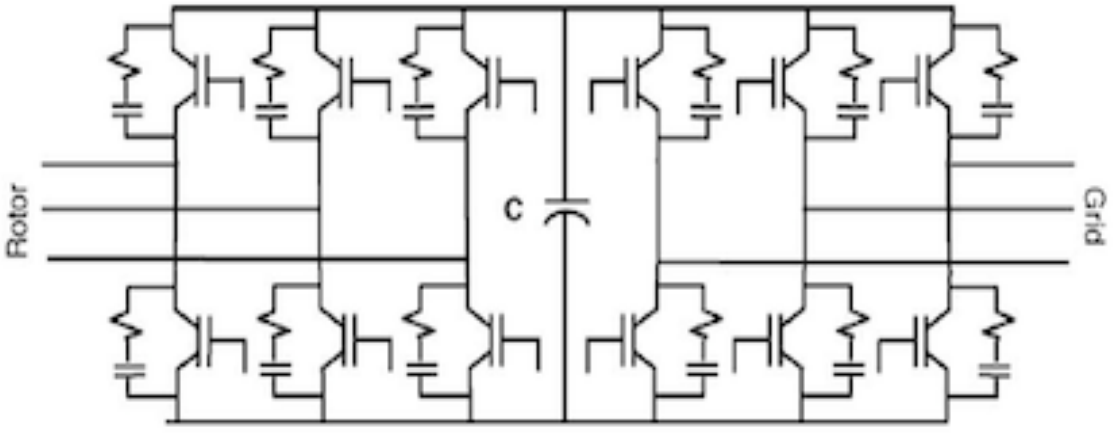

Figure 3-13 DFIG Back-to-Back Converter (Chowdhury and Chellapilla 2005)

is difficult and would have to be done with a digital signal processor, similar to the one used in the diesel generator controller. We derived an algorithm, based on a paper by B. H. Chowdhury (Chowdhury and Chellapilla 2005), to control the back-to-back converter, using an encoder and current sensors, as follows:

Rotor-side Vector Control:

1. Measure stator and rotor currents.
2. Convert these currents into the α-β reference frame.
3. Use the α-β currents to calculate the stator flux angle.
4. The active power set point and the available active power from the machine (i.e. the power being generated by the machine) are input to a P-I loop. The output is the q-axis rotor current.
5. The reactive power set point (set to zero) and the available reactive power from the machine (i.e. the reactive power being generated by the machine) are input to a P-I loop. The output is the d-axis rotor current.
6. The d-q axis currents are converted to the α-β reference frame using the stator flux angle calculated earlier.
7. The α-β currents are converted to a-b-c components.
8. The a-b-c components are used in a state vector modulation or hysteresis modulation scheme to generate gating signals for the rotor side converter.

Stator-side Vector Control:

1. Convert the grid side supply voltages into the α-β reference frame.
2. Calculate the supply angle.

3. Use the voltage across the DC link capacitor and its setpoint value to generate an error signal.
4. Feed the error signal to a P-I loop to get the d-axis current.
5. The q-axis current is forced to zero.
6. Convert the d-q axis currents to α-β frame using the voltage angle.
7. Convert the α-β currents to a-b-c frame.
8. Use state vector modulation or hysteresis modulation to generate gating signals for the supply side converter.

Successful implementation of this algorithm will produce a fully operational doubly fed induction generator. Many of the components required to implement this scheme have already been purchased and can be found in the project work area.

4. Loads

There are currently five different types of load in our system: resistive, capacitive, phase-controlled resistive, inductive, and induction motor. Our electromechanical relay switching system allows us to connect and disconnect the loads arbitrarily from the live microgrid bus, enabling rapid changes in load on the system. The individual loads are described in this section.

4.1 Resistive Load

There are currently two resistive loads in our system, consisting of six ceramic power resistors capable of high current and high temperature operation. The resistors are bolted to a large metal plate mounted at the top of the load side of the project board.

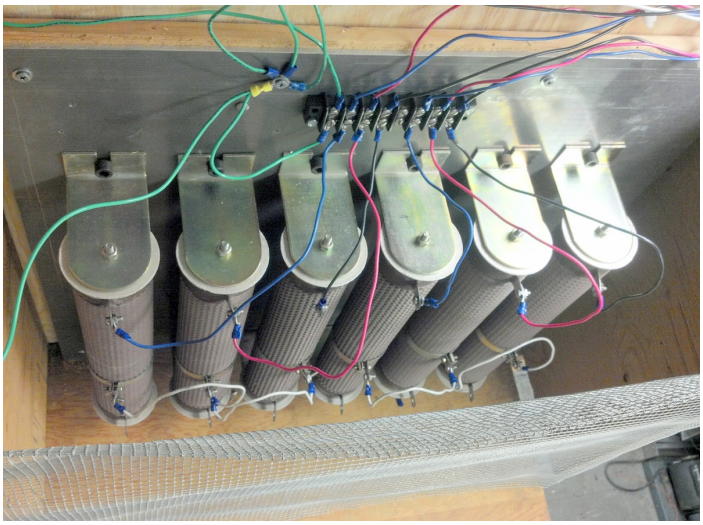

Figure 4-1 Resistive Load

The resistors and metal mounting plate are protected from accidental contact by two wooden side panels and a grounded wire screen. Each resistor has three connection points: one connection on each end and an adjustable band that allows the resistors to be tuned to an arbitrary resistance between 0 ohms and approximately 72 ohms. With these available connection points, it would be simple to connect the six resistors in any series or parallel combination of Y or delta configurations. There is a terminal strip at the top of the metal mounting plate that provides three-phase connections to

the first and second electromechanical relays (counting from the top of the board) on the bus side of the project board, but there is currently no neutral wire connected to this terminal strip.

Each resistor is currently tuned to 48 ohms. At a nominal system voltage of 120 V_{RMS}, this tuning yields a power dissipation of 300 watts per resistor or 900 watts per resistor array. With two resistor arrays, this allows us up to 1800 watts of resistive load on the system. If the resistors are tuned to higher power levels, care should be taken that the extra heat generated does not exceed the temperature rating of the wire insulation, or else the mounting board should be rotated so that the terminal strip and wires are below the resistive loads.

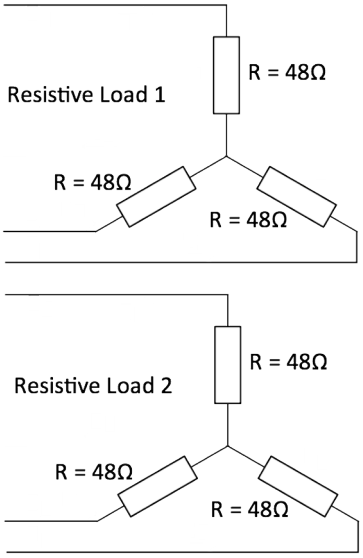

Figure 4-2 Resistive Load Diagram

4.2 Capacitive Load

The capacitive load consists of six AC motor-start capacitors. The capacitors are mounted in an aluminum case at the top of the load side of the project board, to the left of the resistive load. There is currently no protective covering over this load as it is mounted high enough on the board to be out of the range of accidental contact. Each capacitor has two four-lead connection points, which we connected to the system using 0.25-inch quick connect/disconnect terminal connectors. With these available connection points, it would be simple to connect the six capacitors in any series or parallel combination of

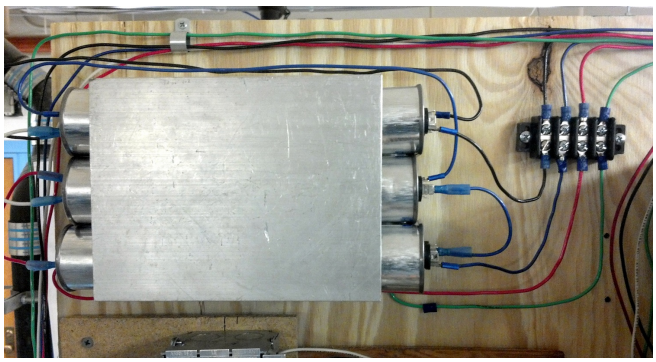

Figure 4-3 Capacitive Load

Y or delta configurations. There is a terminal strip to the right of the capacitive load that provides access to the third electromechanical relay on the bus side of the project board, but there is currently no neutral wire connected to this terminal strip.

Each capacitor in the load is approximately 80µF. In their current configuration, the capacitors are connected in a Y arrangement with the neutral point unconnected. Each leg of this array consists of two capacitors in series, yielding an equivalent capacitance of 40µF per leg. At a nominal system voltage of 120 V_{RMS}, this configuration yields a reactive power of around 217 VAR per capacitor into the system or around 651 VAR into the system for the entire load. Relatively easy changes in connections can yield several different levels of load, but it is not possible to tune the power level of the capacitive load as finely as the resistive load; however, at the time of writing, there are several smaller motor-start capacitors in the project work area that could be added to the capacitive load to yield intermediate power levels.

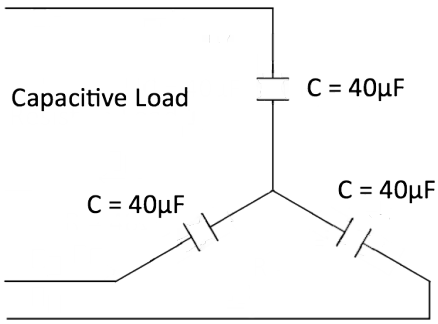

Figure 4-4 Capacitive Load Diagram

4.3 Phase-controlled Resistive Load

The phase-controlled resistive load consists of three light bulbs connected through three residential dimmer switches. This load is mounted at the top left of the load side of the

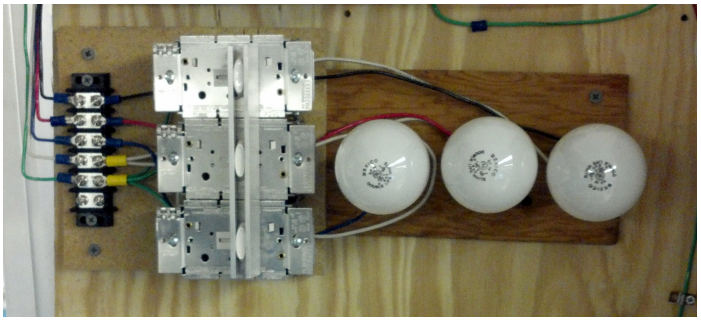

Figure 4-5 Phase-controlled Resistive Load

project board, below the capacitive load and to the left of the resistive load. The dimmer switches are mounted on a separate board from the light bulbs so that the load connected to the dimmer switches can be changed in the future, if so desired. There is no protective covering over this load as most of the connections are completely enclosed and access to the dimmer switches is necessary if the power level is to be changed. We mounted the three dimmer switch boxes in parallel and constructed a metal bar connecting the three dimmer toggles, thereby allowing us to adjust the level of all three dimmer switches evenly. This bar is removable if an unbalanced load is desired. There is a terminal strip to the left of the load, mounted on the same board as the dimmer switches, which provides a connection to the fourth electromechanical relay on the bus side of the project board.

Operating at a nominal system voltage of 120 V_{RMS}, the light bulbs in this load are 60 watts each, providing a total resistive load of 180 watts. These light bulbs are connected in a Y configuration with the neutral point connected to the microgrid bus neutral. Each dimmer switch is connected in series with the live wire of its corresponding light bulb, and each dimmer is capable of full range dimming, from 0% to 100%.

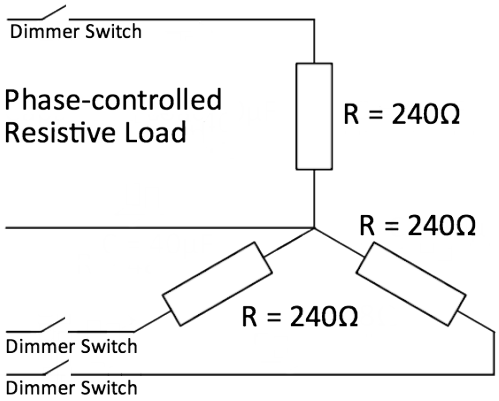

Figure 4-6 Phase-controlled Resistive Load Diagram

4.4 Inductive Load

The inductive load consists of three hand-wrapped inductors. These inductors are mounted on the top shelf on the load side of the project board, between the three-phase power outlet and the resistive load. We built a protective case for this load that consists of a

three-sided wooden frame with the other three sides covered by a grounded wire screen. This allows the inductors to receive proper ventilation without the chance of accidental contact with electrical or thermal hazards. There is a terminal strip on the back of the protective case that provides a connection to the fifth electromechanical relay (counting from the top of the board) on the bus side of the project board.

Figure 4-7 Inductive Load

The inductors were constructed using three split, laminated iron cores. Each inductor has a winding consisting of around 270 turns of 14-gauge magnetic wire wrapped around a rectangular plastic bobbin. Since we were working with a split core, we were able to place the wire-wrapped bobbin on one half of the core and then use appropriately sized pieces of FR-4 glass-epoxy laminate sheeting to maintain a constant gap size between the halves of the iron core. With the bobbin on the core and the FR-4 maintaining the gap size, we used worm-gear hose clamps to keep the two halves of the iron core pressed together. Constructed in this way, we were able to build three inductors of around 108mH each, which we connected in a Y configuration with the neutral point connected to the microgrid bus neutral. At a nominal system voltage of 120 V_{RMS}, this

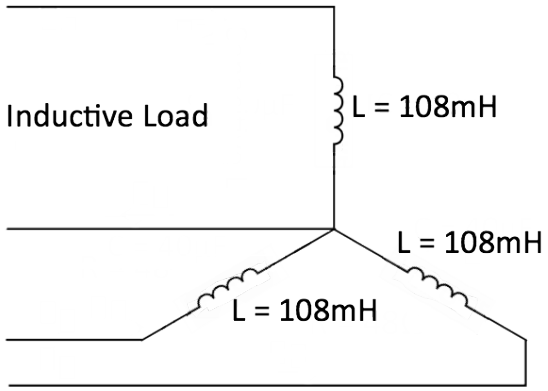

Figure 4-8 Inductive Load Diagram

configuration yields a reactive power of around 354 VAR per inductor out of the system or around 1061 VAR out of the system for the entire load. If smaller or larger load is desired, the gap size of each inductor can be adjusted to raise or lower the inductance within small bounds, or else more turns can be added to or removed from each winding.

4.5 Induction Motor Load

The induction motor load in our system consists of a 0.75-horsepower squirrel-cage induction motor mechanically coupled to a 1.5-horsepower separately excited DC motor. The two motors are bolted to a heavy steel base under the table on the load side of the project board. To get the shafts to align for a proper coupling, we mounted the DC motor directly to the steel base but used aluminum shims to raise the smaller induction motor to the appropriate height. We coupled the shafts with the same Lovejoy jaw coupling described in the diesel generator section above, again boring out the 22mm inner diameter to fit the 7/8-inch motor shafts. The induction motor is electrically connected to the sixth electromechanical relay (counting from the top of the board) on the bus side of the project board. To have an adjustable load on the induction motor, we connected a power resistor across the armature of the DC motor and connected an adjustable DC power supply across the field of the DC motor. The power resistor is mounted inside a wood and wire screening enclosure to the left of the induction motor load, under the table on the load side of

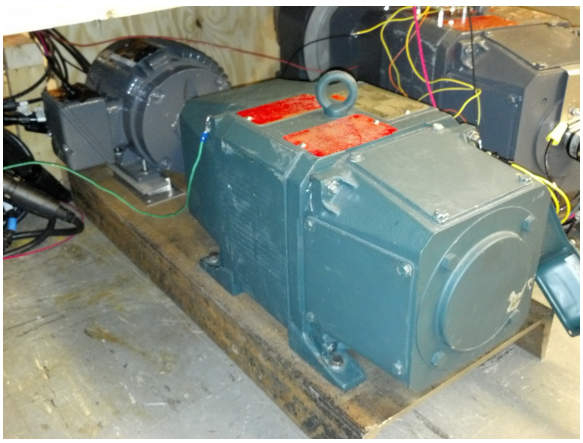

Figure 4-9 Squirrel-cage Induction Motor and DC Motor Set

the project board. The DC power supply connected to the field of the DC motor currently sits on top of the table on the load side of the project board.

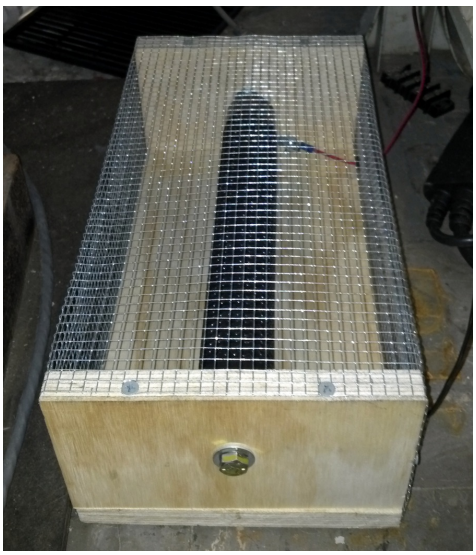

Figure 4-10 DC Motor Power Resistor

By adjusting the DC power supply connected to the field of the DC motor, we can achieve an adjustable mechanical load on the induction motor. This is possible because the power dissipated by the resistor on the armature of the DC motor, and by approximation, the mechanical power dissipated by the induction motor, is described by the equation:

$$P_{diss} = \frac{E_a^2}{R_a}$$

where E_a is the generated voltage in the armature and R_a is approximately the resistance of the resistor connected to the armature, which is 50 ohms. The generated voltage is related to the field voltage by the equation:

$$E_a = \Omega \cdot M \cdot I_f = \Omega \cdot M \cdot \frac{V_f}{R_f}$$

for slowly varying field currents, I_f, where Ω is the mechanical speed of the shaft, M is the mutual inductance between the armature and field, V_f is the field voltage, and R_f is the field resistance. We can then describe the power dissipation as a function of field voltage with the equation:

$$P_{diss} = \frac{\left(\Omega \cdot M \cdot \frac{V_f}{R_f}\right)^2}{R_a}$$

Operating in this configuration, the no-load current (where V_f = 0) drawn by the induction motor is approximately 1.92 amperes at a nominal voltage of 208 $V_{RMS,line-line}$. Note that even with no voltage applied to the field of the DC motor, there may still be current flowing in the armature power resistor due to residual magnetism in the motor iron. The induction motor reaches its rated current of 3.4 amperes with an applied DC motor field voltage of approximately 185 volts. The power supply currently used for the field excitation is a Matsusada RE500-2.4-LUs1, which is capable of outputting 2.4 amperes at 500 volts, so care should be taken not to greatly exceed the ratings of the machines. This power supply also has a USB control module installed, which allows us to control the output of the supply using any desktop computer, if this is desired. We wrote a basic program in C++, saved on the project computer, which allows us to cycle through a vector of voltage values with an arbitrary delay between values, but this is not currently in use and the voltage is simply set by the knob on the power supply.

Using IEEE Standard 112, we found the parameters of the induction motor load to be the following, where the parameters in the table refer to the circuit elements in the accompanying schematic:

X_1	3.08Ω
X_2	3.08Ω
X_m	64.0Ω
R_1	2.65Ω
R_2	1.24Ω
R_c	362Ω

Figure 4-12 Induction Motor Parameters

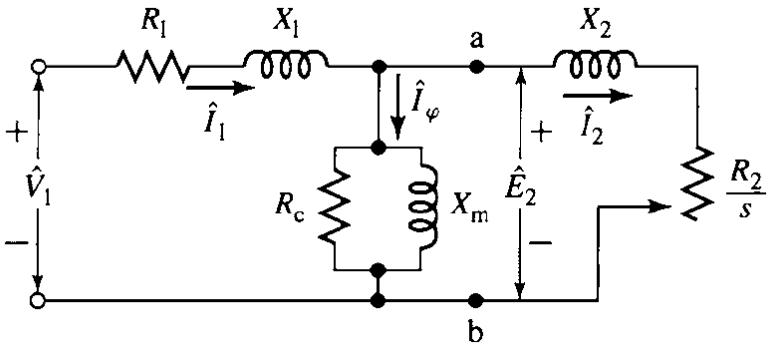

Figure 4-11 Squirrel-cage Induction Motor Single Phase Equivalent Circuit (Fitzgerald, Kingsley and Umans 2003)

Using IEEE Standard 113, we found the parameters of the DC motor to be the following:

Armature Resistance	0.7Ω
Armature Inductance	0.032H
Field Resistance	275Ω
Field Inductance	7.5H
Armature to Field Mutual Inductance	2.97H

The current, voltage, power, and speed ratings for the machines are clearly labeled on the machine nameplates.

5. Switching System

The switching system is an essential part of the project that allows us to dictate which specific loads and generators will be connected at any given time. We can also use the switching system to create an intentional fault on our system, as well as to connect and disconnect the microgrid to the central utility. To perform all of these operations, we used both magnetic contactor relays and solid-state relays.

5.1 Magnetic Contactor Relays

For the ability to individually switch on and off each of the loads, general-purpose magnetic contactor industrial relays were used. These relays are normally open and get switched on when a 24VDC supply sourcing 18mA is connected across the coil terminals. This on/off signal is supplied in our system by the white and yellow wires from the switch drivers. For a visual indication that the switch is powered on, a red LED is placed in series with a 24-kΩ resistor. When there is 24 volts across the coil terminals, the switch is closed and the red LED is illuminated. The relays are rated up to 25 amperes at full load and 30 amperes for a fully resistive load.

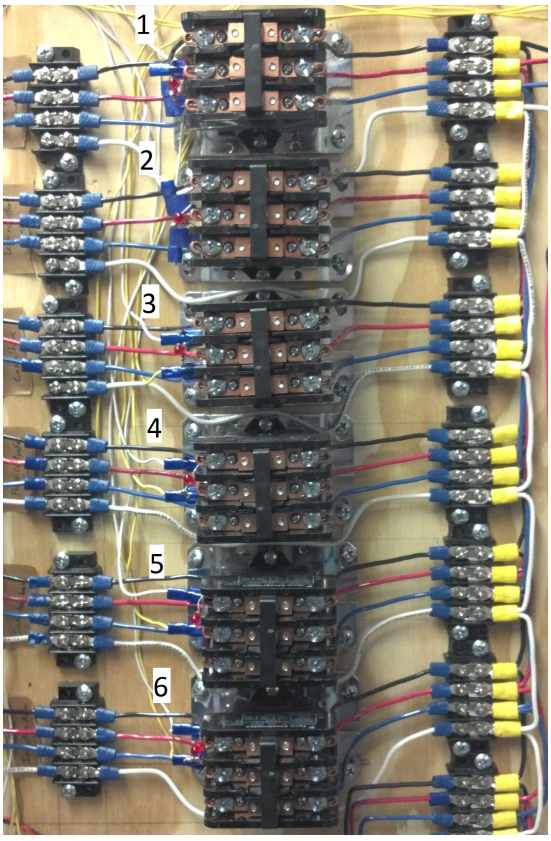

Figure 5-1 Load Relays

There are currently seven of these general-purpose industrial relays being used on the project, six of which are used to connect the microgrid bus to the various loads.

Relay #	Connects microgrid bus to:
1	Right Resistor Load
2	Left Resistor Load
3	Capacitor Load
4	Phase-Controlled Load
5	Inductor Load
6	Induction Motor Load

The seventh general-purpose industrial relay is being used as the faulting switch and has the utility on one side and the microgrid bus on the other side. This relay has a custom shorting bar (seen on the right of the switch in Figure 5-2) that can be placed across all three phases of the switch. When this switch is closed with the shorting bar in place, it will induce a three-phase line-to-line symmetric fault.

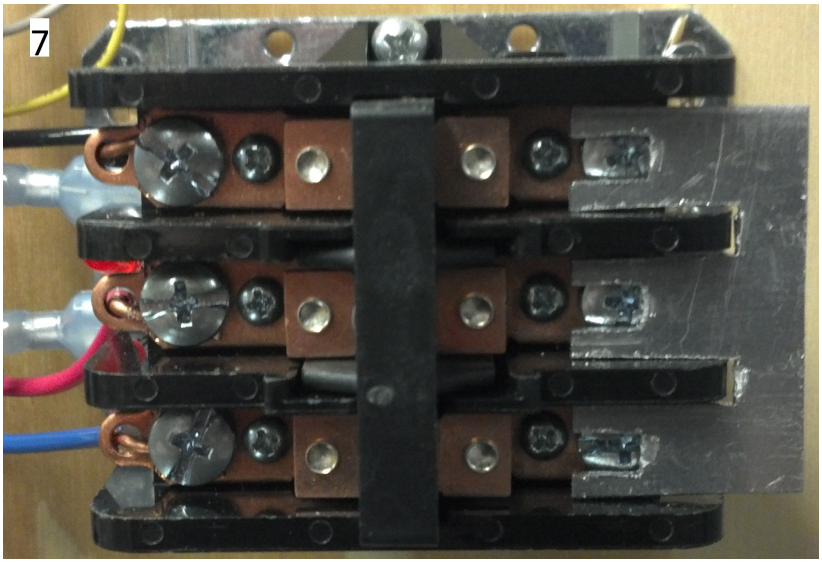

Figure 5-2 Shorting Relay

5.2 Solid State Relays

Along with the seven magnetic contactor relays, there are four solid-state relays being used on the microgrid. The solid-state relays are rated up to $480V_{RMS}$ and $55A_{RMS}$ with a built-in LED status indicator. The solid-state relays also have their on/off signal connected in our

system by the white and yellow wires from the switch drivers and are switched on with 24 volts. The first three solid-state relays (pictured to the right) all switch on the various generators and connect them to the microgrid, as shown below:

Solid State Relay #	Connects microgrid to:
1	Solar Farm Generator
2	Wind Farm (in the future)
3	Diesel Generator

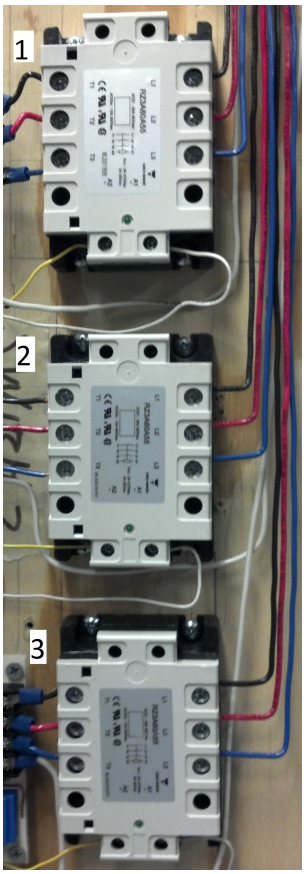

Figure 5-3 SSR Generator Relays

The fourth solid-state relay connects the three-phase microgrid bus to the three phases of the utility. This is the solid-state relay that will be in the open state when the microgrid is in the islanded condition. This is also the switch that needs to be closed at the proper time to synchronize the microgrid with the utility. As shown in Figure 5-4, there are two 12-watt 120VAC light bulbs in series across each phase, which will be illuminated with the switch open to indicate that the microgrid and utility are not synchronized.

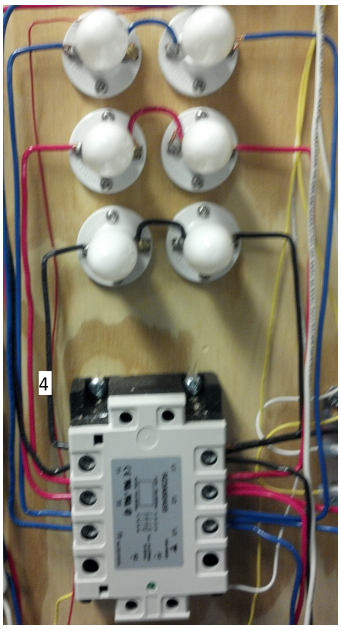

Figure 5-4 SSR Microgrid-Utility Relay

5.3 Driving Boards

In order to be able to control the on/off state of the relays from the computer, we used a National Instrument Multifunctional Data Acquisition System (DAQ). The NI USB-6008 has 12 TTL outputs, which we used to control the relays; however, the +5 volt (TTL logic) is not the 24 volts required to trigger on and off the

relays. To remedy this, we built driving boards to properly amplify the 5 volts to the required 24 volts for the switching.

5.3.1 Magnetic Contactor Relay

For the magnetic contactor relays, we designed a driving board with seven basic common emitter BJTs. For this circuit, as shown in Figure 5-5, with the BJT in cut-off, there is close to 0 volts across the coil terminals such that the relay is in the OFF state. When there is a 5 volt input from the DAQ, there is an 810-ohm resistor at the base of the BJT to provide current to turn on the device. With 5 volts being outputted from the DAQ, and an inherent voltage across the internal diode in the BJT between the base and the collector of around .7 volts, we expect $\frac{5\ volts - .7\ volts}{810\ ohms} \approx 5.3\ milliamperes$ which will turn the BJT on and make it approximately a short. With the switch in the ON state, there will be close to the full 24 volts across the coil terminals and it will thus be in the ON state as well. Note that a diode was placed in the reverse direction across the coil terminals to behave as a freewheeling diode in the case when the device is switched off. When switched off, the inductive coil cannot support a sudden change in current without imposing a large voltage because for an inductor, $V_L = L * \frac{di_L}{dt}$, so the freewheeling diode will help circulate current to minimize the strain on the BJT when switching.

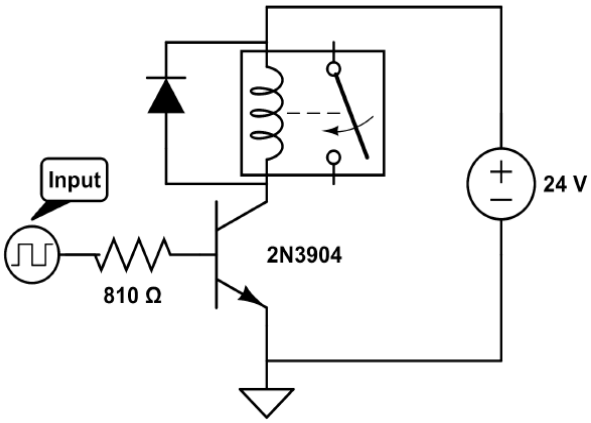

Figure 5-5 Circuit Diagram of Magnetic Contactor Relay Driving Board (1 of 7)

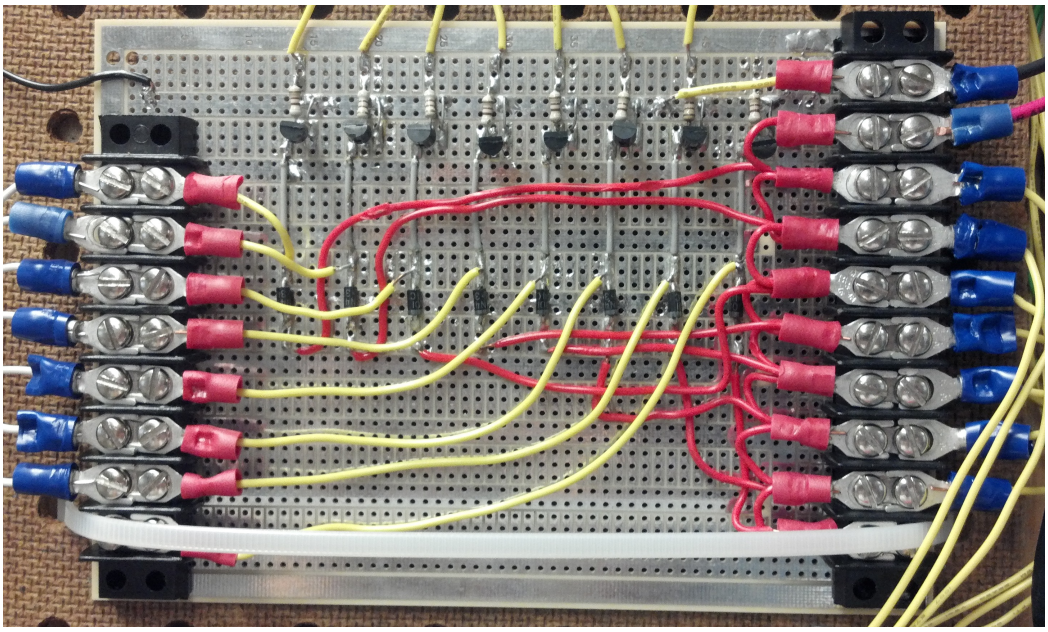

Figure 5-6 Magnetic Contactor Relay Driver Board

5.3.2 Solid State Relay

Like the magnetic contactor relay driving board, there are four standard common emitter BJTs used for the amplifier circuit on the driving boards for the solid-state relays (SSR). The predominant difference between the two boards is that the SSR input terminal has a small impedance but requires the entire 24 volts across it to turn on. If it were placed by itself in series with the BJT, there would be a voltage divider between its impedance and the impedance of the BJT that would prevent the full 24 volts from appearing across the SSR input terminals. Therefore, the SSR input terminals were put in parallel with a large resistor of 13000 ohms and now it has close to the full 24 volts across it when the BJT is in the ON state.

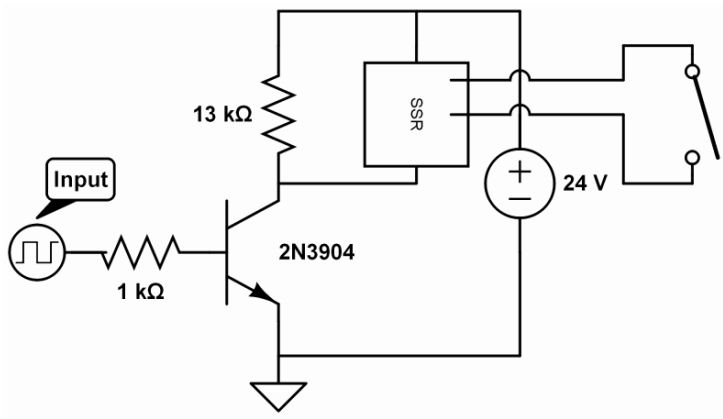

Figure 5-7 Circuit Diagram of the Solid State Relay Driver Board (1 of 4)

Additionally, the 13000-ohm resistor acts as a pull-up resistor to prevent the lower input terminal from floating in the BJT OFF state. For the BJT to be in an ON state, the DAQ outputs 5 volts, which when put across the 1000-ohm resistor to the .7 volts on the base of the BJT, results in a similar ≈ 5 milliamperes.

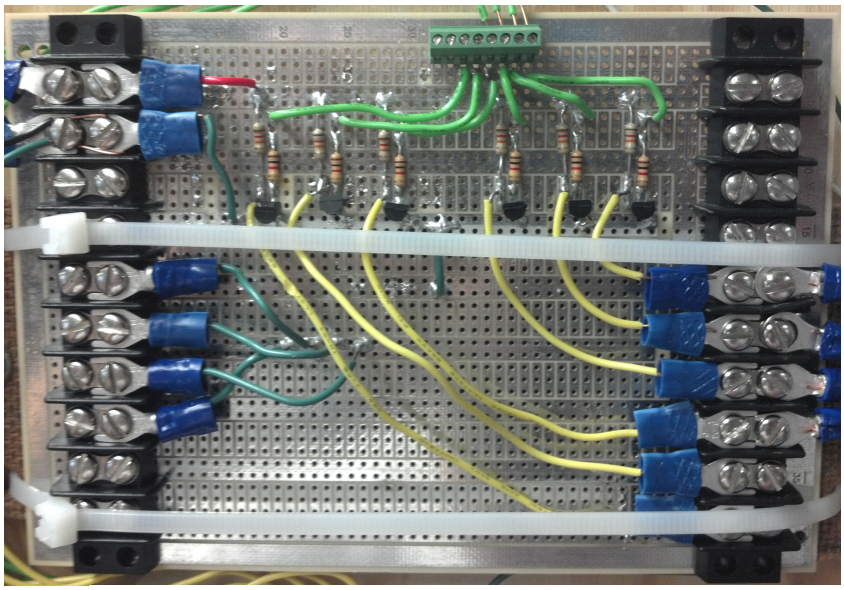

Figure 5-8 Solid State Relay Driver Board

5.4 Faulting System

One of the most important tests we want to perform on the microgrid is to see how the microgrid behaves during islanding conditions. The most important of these islanding conditions is when the microgrid is disconnected from the central utility because of a fault on the utility. Without an easy way to properly simulate a fault, we will actually impose a three-phase line-to-line symmetric fault on our system. It is important to note that during the fault, none of the lines are shorted to neutral or ground.

5.4.1 Faulting Bar

In order to induce a fault, we have constructed a faulting bar that is mounted onto the seventh mechanical contactor relay. This is just a piece of aluminum that was machined into an "E" shape (see Figure 5-9) to fit the terminals of the relay. While we are interested in measuring and observing the effects that this fault will have on the system, there are a few things that we expect to happen. Once the seventh mechanical contactor relay is engaged and the fault is induced, we expect the fourth solid-state relay to trip and become an open after a few cycles. Once this is opened, the microgrid will be in the islanded state. Similarly, it is possible, and probably likely, that the breakers for the three phases in the load center will trip after a few cycles and thus disconnect the fault from the central utility. However, before this fault is disconnected from the central utility, there will be a few cycles with very large current being drawn because of the fault. To help minimize this current, and hopefully prevent the entire lab's lights from dimming too much, we have added some current limiting inductors to the system.

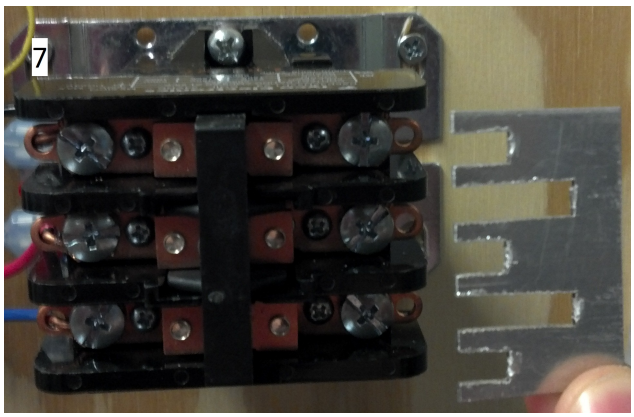

Figure 5-9 Shorting Bar

5.4.2 Current Limiting Inductors

An inductor was placed in series with each phase to provide an impedance for when the three phases are shorted together line-to-line. This impedance limits the current from the utility. Without this series impedance, there would be very little impedance limiting the utility from delivering excessive current until the breaker was flipped a few cycles later. The inductor

fights the surge in current due to the fault to help protect the utility and it also does not dissipate much real power, mostly reactive power. These inductors were constructed using three split, laminated iron cores. Each inductor has a winding of 12-gauge magnetic wire wrapped around a rectangular plastic bobbin that acts as a shield between the wire and the core. This helps with heating and also ensures that the insulation around the magnetic wire is not scraped off from the edges of the inductor. The rectangular bobbin was first wrapped independently and, since we were working with a split core, we were able to place the wire-wrapped bobbin on one half of the core and then use appropriately sized pieces of FR-4 glass-epoxy laminate sheeting to maintain a constant gap size between the halves of the iron core. With the bobbin on the core and the FR-4 maintaining the gap size, we used worm-gear hose clamps to keep the two halves of the iron core pressed together. To size the inductors, we decided that we wanted it to have an impedance of approximately 5 ohms at 60 hertz. The 5 ohms implies that if the 120 volts are shorted across the inductor from a fault, there will be an absolute max of 24 amps flowing through it. $|Z| = 5\ ohms = |j\omega L|$. So to solve for the desired inductance:

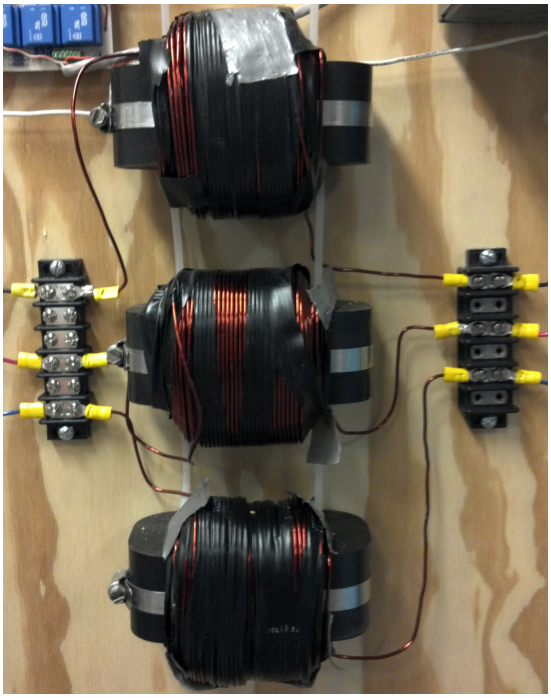

Figure 5-10 Shorting Inductors (all 3 phases)

$$L = \frac{5\ ohms}{2 * \pi * 60\ hertz} = .01326\ henries$$

To determine the required number of turns we would need for this inductance,

$$L = \frac{N*B_{sat}*Area}{I} \; so \; N = \frac{L*I}{B_{sat}*Area}.$$

Upon measuring the core, its cross sectional area was 1 inch by 2 inches and it was determined that we would use a conservative estimate for B_{sat} = 1 Tesla.

$$N = \frac{.01326\ henries * 24\ Amps}{1\ Tesla * 2\ inches^2} \approx 247\ turns$$

Now, to solve for the appropriate gap size (g), we used Ampere's Law:

$$H * 2 * g = N * I$$

We were then able to solve for the appropriate gap size:

$$g = \frac{N * I}{2 * H} = \frac{247\ turns * 24\ Amperes}{2 * \frac{1\ Tesla}{\mu_o}} = 3.725\ mm$$

While we made these calculations, we left additional magnetic wire so that we could add a few turns to have our measurements meet the expected inductance. Additionally, we needed to add some extra FR-4 to increase the gap size. In the end, we used 270 turns and had a gap size around 1.25 cm. When measured on the LCR meter, our series inductors are now the desired 5 ohms. Note that because the inductors are in series with the loads, there is a voltage divider and therefore the loads (when connected) do not have the full 120 volts across them without generation sources supporting the microgrid bus voltage.

5.5 Synchronization

Our microgrid is designed to run both in parallel with the central utility as well as independent of it. A microgrid can be islanded (disconnected) from the central utility because a forced fault caused the breakers connecting the two systems to open or because it was intentionally islanded. Additionally, a microgrid can be intended to run independently of the

central utility. Essentially, disconnecting a microgrid from the central utility is not a difficult problem to solve assuming that the microgrid can support all the loads independently and the voltage and frequency regulation of the system is sufficiently robust. However, the reconnecting of the microgrid back to the central utility can be a very difficult problem to solve. In order to properly reconnect, it is essential that the two systems have nearly identical frequencies in their waveforms and that the three microgrid phases not have a significant phase shift from the corresponding phase of the utility. Additionally, the phases must be rotating in the same direction. The two systems should have similar voltages although it is possible the stronger utility can pull up a drooping microgrid voltage. When these conditions are met, the microgrid and the utility can be synchronized.

5.5.1 Synchronizing Light Bulbs

For our system, we hope to eventually be able to synchronize the microgrid with the utility through the LabVIEW interface. However, we have established a visual method for ensuring that the two systems are properly synchronized before they are reconnected together. Two standard 120-VAC, 7-watt light bulbs were connected in series across the fourth solid-state relay that connects the microgrid with the utility. Two light bulbs were needed instead of one because if the two phases in each system are phase shifted by 180 degrees, there will be a maximum of $240V_{RMS}$ across the bulbs. The light bulbs will be illuminated if there is a voltage across

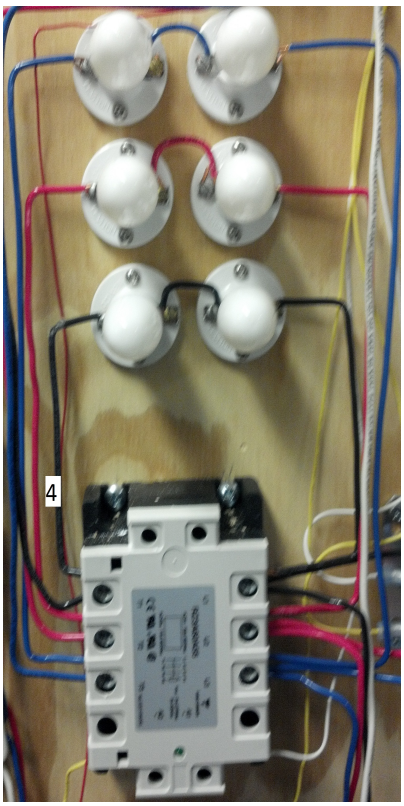

Figure 5-11 Synchronizing Light Bulbs

their terminals: the brighter the bulbs, the higher the voltage. If there is a voltage difference between the microgrid and the utility for a given phase, the light bulbs for that phase will be illuminated thus implying that the system cannot be synchronized. All of the light bulbs must be off, to insure that the system is synchronized, before it is safe to reconnect the microgrid with the central utility.

6. Monitoring System

The monitoring system is an essential part of the project as it allows us to capture data on important variables from experiments for real time visualization. The monitoring system also stores the data, which can later be analyzed. The monitoring system is made up of various National Instruments Data Acquisition (DAQ) devices as well as custom built voltage and current measurement boards.

6.1 DAQs

Currently, there are three DAQs being used on the project, two of the NI USB-6211 variety and one NI USB-6008. The NI USB-6211 has 16 analog inputs, 4 digital inputs, 2 analog outputs and 4 digital outputs each with 16 bits of resolution. The NI USB-6008 has 8 analog inputs, 2 analog outputs and 12 interchangeable digital I/O each with 12 bits of resolution. There will be 6 analog inputs from each measurement board and a digital output for each relay. In the end, just for these applications, we will use a total of 30 analog inputs and 11 digital outputs and therefore need a few DAQs for the microgrid. DAQs 1 and 2 (from top to bottom) connect the measurement boards and their pin-outs can be seen in the measurement boards section. The pin-out for DAQ 3 (the NI USB-6008), which controls the switches, is as follows:

DAQ #3 (Relay Control DAQ)	Wire Color	Connection	I/O	Type
P0.0	Green	SSR1 Driver Board BJT Base	Output	Digital
P0.1	Green	SSR2 Driver Board BJT Base	Output	Digital
P0.2	Green	SSR3 Driver Board BJT Base	Output	Digital
P0.3	Green	SSR4 Driver Board BJT Base	Output	Digital
P0.4	Yellow	MCR1 Driver Board BJT Base	Output	Digital
P0.5	Yellow	MCR2 Driver Board BJT Base	Output	Digital
P0.6	Yellow	MCR3 Driver Board BJT Base	Output	Digital
P0.7	Yellow	MCR4 Driver Board BJT Base	Output	Digital
P1.0	Yellow	MCR5 Driver Board BJT Base	Output	Digital
P1.1	Yellow	MCR6 Driver Board BJT Base	Output	Digital
P1.2	Yellow	MCR7 Driver Board BJT Base	Output	Digital
GND	Green	Ground on Driver Board	Output	Ground

6.2 Measurement Boards

The measurement boards were designed by one of our group members, Jorge Elizondo, to allow for an integrated measurement and analysis of main performance variables such as current and voltage of the system at various targeted nodes. The boards themselves consist of three (one for each phase) Pulse Electronic Corporation Transformers, which take a primary voltage up to 230VAC and output a secondary voltage up to 6 VAC with an approximate turns ratio of 38. These transformers have a large input impedance so that they have a minimal impact on the system they are monitoring. The intention is to get the high line voltage into a range for which it

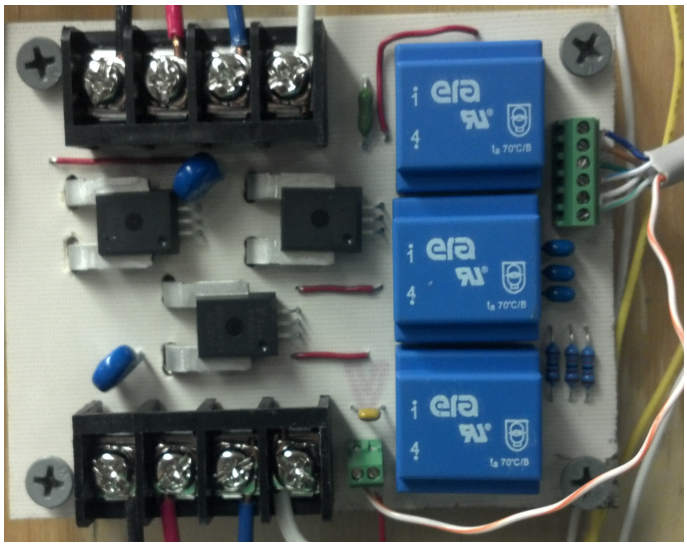

Figure 6-1 Beta Prototype of Measurement Board

is within the tolerance of the input range of the DAQs. There are also three Allegro Current Sensors, which measure the current of each phase of the system and output an analog voltage to the DAQs.

There are fuses on the neutral of the primary side of each transformer to help protect the transformer in the case of a current spike. Additionally, there are EPCOS Inc. Varistors, which will protect the transformers if there is a large spike in line to neutral voltage on any of the phases. At the time of writing, there are currently four measurement boards on the microgrid, with another being built:

Measurement Board #	Measurement Node
1	Diesel Generator Emulator
2	Solar Farm Emulator
3	Utility main grid
4	Microgrid Bus
5*	Wind Turbine Emulator (not shown)

Note that the measurement board on the Wind Turbine Emulator will be added in the future.

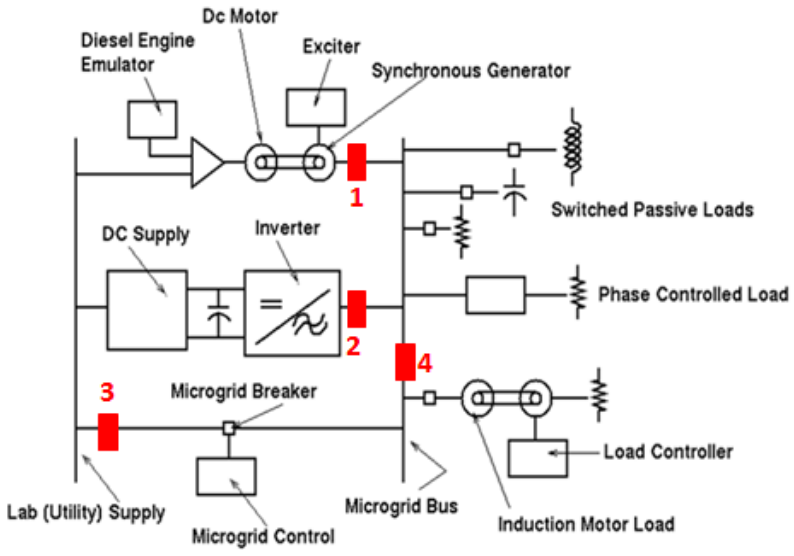

Figure 6-2 Measurement Board Locations

Measurement Board 1 (Diesel Generator)	**Wire Color**	**Connection**	**I/O**	**Type**
V1	Blue	AI0 (DAQ 2)	Output	Analog
V2	Brown	AI1 (DAQ 2)	Output	Analog
V3	Green	AI2 (DAQ 2)	Output	Analog
I1	White/Blue	AI3 (DAQ 2)	Output	Analog
I2	White/Brown	AI4 (DAQ 2)	Output	Analog
I3	White/Green	AI5 (DAQ 2)	Output	Analog
+5V	Red	Supply +5 V	Input	Power
GND	White/Orange	GND (DAQ 2) and Supply V-	Input	Ground

Measurement Board 2 (Solar Farm Emulator)	**Wire Color**	**Connection**	**I/O**	**Type**
V1	Blue	AI6 (DAQ 2)	Output	Analog
V2	Brown	AI7 (DAQ 2)	Output	Analog
V3	Green	AI8 (DAQ 2)	Output	Analog
I1	White/Blue	AI9 (DAQ 2)	Output	Analog
I2	White/Brown	AI10 (DAQ 2)	Output	Analog
I3	White/Green	AI11 (DAQ 2)	Output	Analog
+5V	Red	Supply +5 V	Input	Power
GND	White/Orange	GND (DAQ 2) and Supply V-	Input	Ground

Measurement Board 3 (Utility)	**Wire Color**	**Connection**	**I/O**	**Type**
V1	Blue	AI0 (DAQ 1)	Output	Analog
V2	Brown	AI1 (DAQ 1)	Output	Analog
V3	Green	AI2 (DAQ 1)	Output	Analog
I1	White/Blue	AI3 (DAQ 1)	Output	Analog
I2	White/Brown	AI4 (DAQ 1)	Output	Analog
I3	White/Green	AI5 (DAQ 1)	Output	Analog
+5V	Red	Supply +5 V	Input	Power
GND	White/Orange	GND (DAQ 1) and Supply V-	Input	Ground

Measurement Board 4 (Microgrid Bus)	Wire Color	Connection	I/O	Type
V1	Blue	AI6 (DAQ 1)	Output	Analog
V2	Brown	AI7 (DAQ 1)	Output	Analog
V3	Green	AI8 (DAQ 1)	Output	Analog
I1	White/Blue	AI9 (DAQ 1)	Output	Analog
I2	White/Brown	AI10 (DAQ 1)	Output	Analog
I3	White/Green	AI11 (DAQ 1)	Output	Analog
+5V	Red	Supply +5 V	Input	Power
GND	White/Orange	GND (DAQ 1) and Supply V-	Input	Ground

Note that for each of the measurement boards, the 6 V/I pins are in order from the top of the board to the bottom and the ground pin is to the right of the +5V pin when the board is properly oriented.

6.3 LabVIEW

LabVIEW is installed on the project computer and is the overall monitoring and control software that is used for the microgrid project. Within the current LabVIEW program (version 3.1), there is a page for analyzing the system and one for synchronizing the system. These two pages make up the user interface that is used to control the microgrid. Throughout the program, there is a constant top bar that helps the user navigate between pages and make common selections. The farthest left button is the STOP button that acts as the software emergency stop. When pressed, it will turn off all measurement boards and open all relays. To

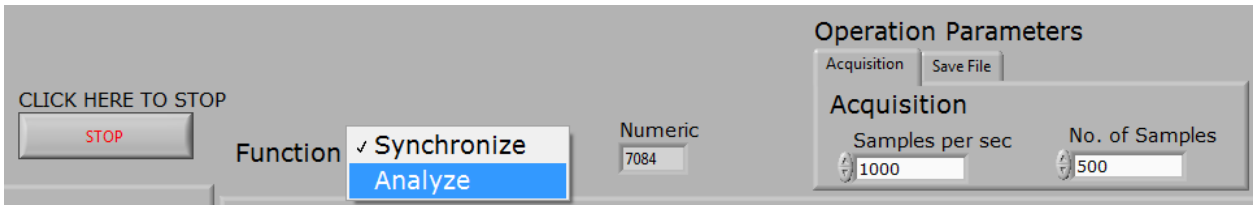

Figure 6-3 LabVIEW Top Control Bar

switch between each of these pages, there is a “Function” tab in the middle of this top bar that, when clicked, shows a drop down menu to select the desired screen. The screen that is checked represents the current screen. There is also the “Numeric” box that acts as a counter for the number of loops the system has performed through the software. Finally, to the right of the top control bar is the Operation Parameters. Within this menu and under the “Acquisition” tab, the user can set the number of Samples per second that each DAQ will collect per channel. Additionally, the user can set the Number of Samples per file. In the current example, the DAQ will collect 1000 samples per second from each channel. After each set of 500 samples, it will process and save the data. Basically, every half-second at 1000 samples per second the DAQ will save and process the data. Under the “Save File” tab, the user can select the location of the file and what to name it as can be seen in the figure. The default is to save the data as a text file.

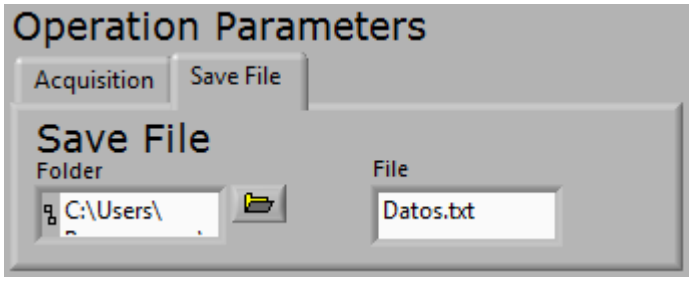

Figure 6-4 LabVIEW "Save File" Tab

In the main section of the screen below the control tab, regardless of whether you are on the “Synchronize” or “Analyze” page, the left of the screen is always occupied by the “SWITCH CONTROL” display. As can be seen from the figure, each relay in the system is represented as a square green button. When clicked by the user, the green button will light up indicating that the relay is closed (in the ON state). Additionally, there is also a circular green button for each measurement board that is illuminated when the measurement board is clicked active. There is also a “Clear all” and “Select all” button that will turn on and off all of the measurement boards. Because the computer has a hard time processing all of the

measurement board data at once, it works best if only the important measurement boards are active during the appropriate test.

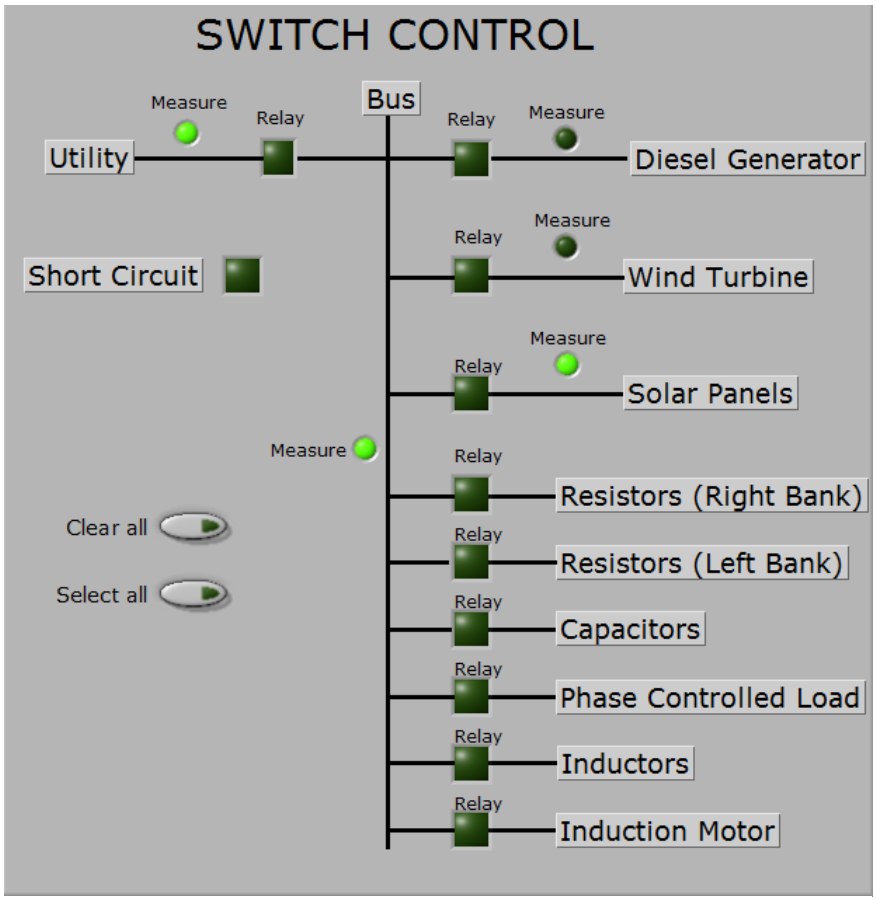

Figure 6-5 LabVIEW Switch Control

The second section of the "Analyze" screen on the LabVIEW program is the measurements section. This section lists all measurements from each measurement board (five total) as a column for each of the voltages (RMS), currents (RMS), voltage phase angles and current phase angles. Within each measurement criterion for each measurement board, there are three values displayed representing the measurement for each phase.

Figure 6-6 LabVIEW Measurements Section

For now, the third section of the "Analyze" page (note it is also the third section of the "Synchronize" page) is the calibration section. This section is more of the back end adjustments that the user can make to change the gains on each measurement that the measurement boards make. This should hopefully be done automatically in the future to calibrate all the sensors and should never need to be adjusted manually.

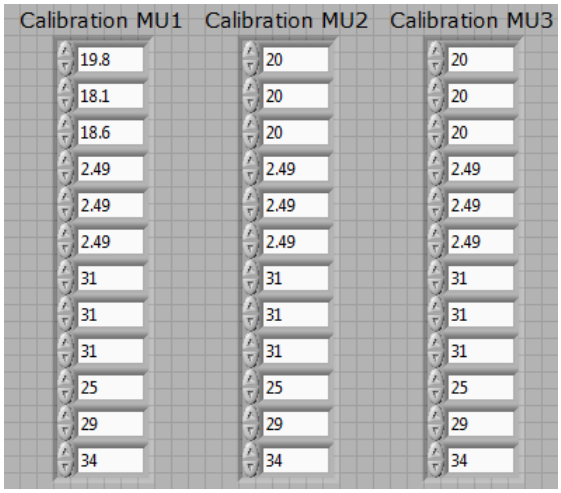

Figure 6-7 LabVIEW Calibration Section

The differentiating section in the

"Synchronize" page is the middle section currently called "Micro-grid points to be synchronized". This section requires you to enable two and only two of the measurement boards from section one and it will clearly display the voltages of each measurement point. In

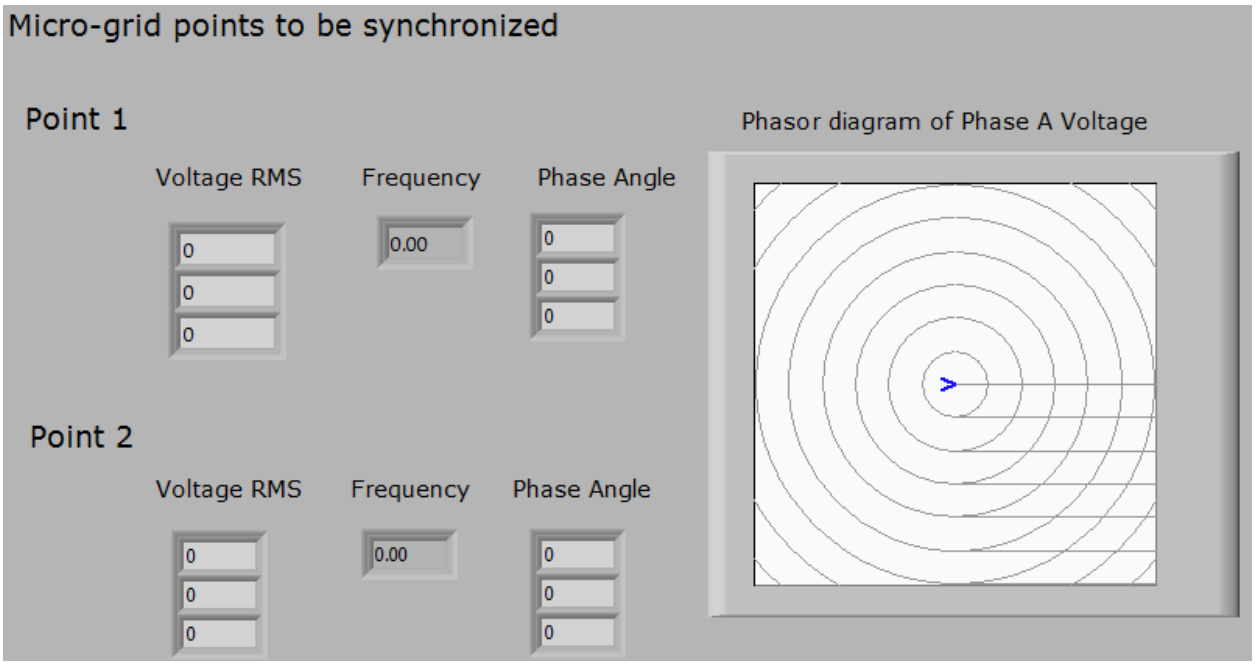

Figure 6-8 LabView Synchronize Page

most cases, the utility will be used as the reference point (Point 1) and the microgrid bus as Point 2. This interface shows the measured frequency and plots a phasor diagram representation of the phase A of each measurement point. If the two points are synchronized, the two blue arrows in the diagram (the lines are not shown in the figure) will overlap.

7. Future Work

This section discusses future work that could improve the present capabilities of the project or implement new systems that expand on current capabilities. The system could be considered complete without the following systems, but these suggestions would all be interesting projects for the system.

7.1 Diesel Generator Excitation System

The present excitation system used on the diesel generator model, as described above, is a rather simple PI controller that sets the voltage on the field based on the difference between the output voltage of the armature of the wound-rotor induction machine and the line voltage of the microgrid bus. This excitation system has the advantage of being simple and easy to implement, but it is far from the optimal control scheme for the system. Developing a more complex excitation system that relies on more than just the output voltage of the generator would help make the system more stable during faults, fault-induced islanding, increases or decreases in load, and other system transients. The dsPIC used to control the DC motor is currently being used well below its full potential and could be very useful in implementing a more complex control scheme.

7.2 Solar Farm Inverter Array

The Enphase microinverters currently used in our system have the advantage of being modular and easy to use; however, they have the major disadvantage of being unable to support voltage independently of other generation sources. The solar farm system could be

improved by replacing these inverters with a six-pack of MOSFETs or IGBTs with associated gate drivers and output filters that could be controlled in a more flexible way than the Enphase microinverters. Such a configuration could implement P-Q droop control or current injection control that would allow the group to study the impact of inverter-based distributed generation on system transients, like faults and fault-induced islanding.

Another improvement in the solar farm system involves changes to the control of the DC power supply. In its present form, the program on the project computer that controls the DC power supply outputs voltage commands that change after a set time interval. A better implementation of this program would give current commands to the power supply instead and would be a more accurate emulation of the electrical characteristics of a photovoltaic cell as it would allow the Enphase inverters to use their built-in maximum power point tracking capabilities.

7.3 Wind Farm

As described in a previous section, some progress has already been made toward constructing a wind farm simulation. This design uses current and voltage measurements as well as an encoder to measure rotor speed and angle. While we believe it would be best to pursue this design and see it to completion before any other design is attempted, a similar design was proposed by a visiting scientist working in our group. This design, which can be found on the project computer, forgoes the use of an encoder and instead uses only current and voltage measurements to implement a doubly fed induction generator. It would be an interesting addition to the project if this second design could also be implemented and the results compared with the original design.

7.4 Induction Motor Load Supply Control

As noted above, the voltage on the field of the DC motor in the induction motor load system is manually controlled by the voltage knob on the supply. However, this power supply is USB controllable, so it would be possible to adapt our simple C++ program on the project computer to implement a more advanced control algorithm that could implement arbitrary load profiles. In this way, it would be possible to implement an induction motor load with periodically varying load that behaves similarly to a refrigerator, on the small scale, or industrial machinery, on a larger scale.

7.5 Microgrid Central Controller

At present, the diesel generator system sets the voltage and frequency of the microgrid bus without any input from the utility bus or other generation sources. After the completion of the wind farm generator and any upgrade of the solar array, it would be a beneficial and interesting project to implement a central control system for the microgrid bus that better coordinates the generation sources with the utility bus. Such a system has the potential to improve the stability of the microgrid during transients like faults and fault-induced islanding.

7.6 Load-shedding Scheme

As described previously, the present system for controlling the load switches is fairly simple. The switch driving board is controlled by the project computer through a DAC, and our LabVIEW interface consists of a few buttons that are either on or off. As a result, a load is either connected to the system or it is not, and switching the state of any particular load must be done by manually clicking the corresponding button. It would be an interesting addition to the

project to implement a load-shedding scheme in LabVIEW that could selectively disconnect and reconnect loads during and after faults and other transients. Nearly all of the required hardware is already in place for this system, and our current LabVIEW control interface would be ideal for implementing a load-shedding algorithm.

Bibliography

Alaboudy, A. H. Kasem, H. H. Zeineldin, and J. Kirtley. "A Simple Control Strategy for Inverter Based DG to Enhance Microgrid Stability in the Presence of Induction Motor Loads." Masdar Institute.

Chowdhury, Badrul H., and Srinivas Chellapilla. "Double-Fed Induction Generator Control for Variable Speed Wind Power Generation." *Electric Power Systems Research*, no. 76 (2005): 786-800.

Fitzgerald, A. E., Charles Kingsley, and Stephen D. Umans. *Electric Machinery.* 6th Edition. New York: McGraw-Hill, 2003.

IEEE Power Engineering Society. *Standard 112 - IEEE Standard Test Procedure for Polyphase Induction Motors and Generators.* The Institute of Electrical and Electronics Engineers, Inc., 2004.

IEEE Power Engineering Society. *Standard 113 - IEEE Guide: Test Procedures for Direct-Current Machines.* The Institute of Electrical and Electronics Engineers, Inc., 1985.

National Renewable Energy Laboratory. "Oahu Solar Measurement Grid." *NREL.* 2011. http://www.nrel.gov/midc/oahu_archive/ (accessed March 29, 2012).

Appendix A – Part Numbers and Datasheets

This appendix lists useful information about the specific hardware used in each section above and lists links to datasheets and other useful documents.

A.1 System Overview

	Part	Manufacturer	Part Number
	Load Center	Square D	QO320L125GRB
Datasheet	http://products.schneider-electric.us/products-services/product-detail/?event=datasheet&partnumber=QO320L125GRB&countrycode=us		
	Breakers	Square D	QO310
Datasheet	http://products.schneider-electric.us/products-services/product-detail/?event=datasheet&partnumber=QO310&countrycode=us		
	Emergency Shutoff Switch	Square D	D-321N
Datasheet	http://products.schneider-electric.us/products-services/product-detail/?event=datasheet&partnumber=D321N&countrycode=us		
	Desktop Computer	HP	505B
Datasheet	http://h10010.www1.hp.com/wwpc/pscmisc/vac/us/product_pdfs/HP_505B_BusinessPC_Datasheet_Sept2010.pdf		
	Voltage Regulator	APC	Pro 700
Datasheet	http://www.apcmedia.com/salestools/DFAH-8GLRDV_R0_EN.pdf		

A.2 Generators

A.2.1 Diesel Generator

	Part	Manufacturer	Part Number
	DC Motor	Reliance	DC0189ATY
Datasheet	http://www.reliance.com/prodserv/motgen/motinfcnt.htm		
	Induction Motor	Reuland	7660466-1
Datasheet	http://reuland.com/Brochures/Wound%20Rotor%20Motor.pdf		
	Current Sensor	Allegro MicroSystems	ACS712ELC-05B-T
Datasheet	http://www.allegromicro.com/en/Products/Part_Numbers/0712/0712.pdf		
	Encoder	Red Lion	ZPJ2500
Datasheet	http://www.redlion.net/Products/Groups/Thru-BoreEncoders/ZPJ/Docs/11033.pdf		

	Part	Manufacturer	Part Number
	Encoder Bore Sleeve	Red Lion	RPGBIM01
Datasheet	http://www.redlion.net/Products/Groups/Thru-BoreEncoders/ZPJ/Docs/11033.pdf		
	Digital Signal Processor	Microchip	dsPICDEM MC1
Datasheet	http://ww1.microchip.com/downloads/en/DeviceDoc/70119E.pdf		
	Coupling	Lovejoy	L075-22mm
Datasheet	http://www.lovejoy-inc.com/products/jaw-type-couplings.aspx		
	Coupling Insert	Lovejoy	68514410621
Datasheet	http://www.lovejoy-inc.com/products/jaw-type-couplings.aspx		
	dsPICDEM MC1 Motor Control Development Board	Microchip	DM300020
Datasheet	http://ww1.microchip.com/downloads/en/DeviceDoc/70098A.pdf		
	6 position Connection Housing	Molex Connector Corporation	WM4267-ND
Datasheet	http://www.molex.com/pdm_docs/sd/050579506_sd.pdf		
	Crimps	Molex Connector Corporation	WM2510-ND
Datasheet	http://www.molex.com/pdm_docs/sd/016020102_sd.pdf		
	16 position Connection Housing	Molex Connector Corporation	WM2525
Datasheet	http://www.molex.com/pdm_docs/sd/022552161_sd.pdf		
	Butt Splice Nylon	Panduit Corporation	298-9995-ND
Datasheet	http://www.panduit.com/groups/MPM-NL/documents/PartDrawing/076693.pdf		

A.2.2 Solar Farm

	Part	Manufacturer	Part Number
	Microinverter	Enphase	D380-72-2LL-S12
Datasheet	http://enphase.com/wp-uploads/enphase.com/2011/03/Enphase_D380_Datasheet.pdf		
	MC4 Cables	Wholesale Solar	9991075
Datasheet	http://www.wholesalesolar.com/products.folder/cable-folder/mc4-extension-cables.html		
	AC Branch Cable	Enphase	ET3C-G2-06
Datasheet	http://enphase.com/wp-uploads/enphase.com/2011/05/Enphase_Field_Wiring_Diagram_D380_208v.pdf		
	DC Power Supply	Matsusada	RE45-45-LUs1
Datasheet	http://www.matsusada.com/pdf/RE.pdf		

A.2.3 Wind Farm

	Part	Manufacturer	Part Number
	Inverter	Powerex	PM30CSJ060
Datasheet	www.pwrx.com/pwrx/docs/pm30csj060.pdf		
	Current Sensor	Allegro MicroSystems	ACS712ELC-05B-T
Datasheet	http://www.allegromicro.com/en/Products/Part_Numbers/0712/0712.pdf		
	Encoder	US Digital	E3-1024-875-I-H-T-B
Datasheet	http://www.usdigital.com/assets/general/76_e3_datasheet_3.pdf		
	Coupling	Lovejoy	L075-22mm
Datasheet	http://www.lovejoy-inc.com/products/jaw-type-couplings.aspx		
	Coupling Insert	Lovejoy	68514410621
Datasheet	http://www.lovejoy-inc.com/products/jaw-type-couplings.aspx		

A.3 Loads

A.3.1 Resistive Load

	Part	Manufacturer	Part Number
	Resistor	Milwaukee Resistor Corp.	8/91
Datasheet	http://www.milwaukeeresistor.com/pdf/roundwire.pdf		

A.3.2 Capacitive Load

	Part	Manufacturer	Part Number
	Capacitor	GE / Genteq	97F9391
Datasheet	http://www.richardsonrfpd.com/resources/RellDocuments/SYS_6/GEC001-MotorRun20080618.pdf		

A.3.3 Phase-controlled Resistive Load

	Part	Manufacturer	Part Number
	Dimmer Switch	Lutron	GL-600P-WH
Datasheet	http://www.lutron.com/TechnicalDocumentLibrary/Spec%20Guide%20Volume%201%20Glyder.pdf		

A.3.4 Induction Motor Load

	Part	Manufacturer	Part Number
	DC Motor	Reliance	DC0189ATY
Datasheet	http://www.reliance.com/prodserv/motgen/motinfcnt.htm		
	Induction Motor	Marathon Electric	143TTFS8026AB W
Datasheet	http://www.marathonelectric.com/MMPS/details.jsp?item=056T17F5322		

	Part	Manufacturer	Part Number
	DC Power Supply	Matsusada	RE500-2.4-LUs1
Datasheet	http://www.matsusada.com/pdf/RE.pdf		
	Resistor	Milwaukee Resistor Corp.	4/98
Datasheet	http://www.milwaukeeresistor.com/pdf/ribwound.pdf		
	Coupling	Lovejoy	L075-22mm
Datasheet	http://www.lovejoy-inc.com/products/jaw-type-couplings.aspx		
	Coupling Insert	Lovejoy	68514410621
Datasheet	http://www.lovejoy-inc.com/products/jaw-type-couplings.aspx		

A.4 Switching System

	Part	Manufacturer	Part Number
	Electromechanical Switch	TE Connectivity	P25P42D22P1-24
Datasheet	http://www.te.com/catalog/pn/en/2-1393132-6?RQPN=P25P42D22P1-24		
	Solid-state Switch	Carlo Gavazzi	RZ3A60D75P
Datasheet	http://www.gavazzionline.com/pdf/RZ3A.pdf		
	BJT	Fairchild Semiconductor	2N3904
Datasheet	http://www.fairchildsemi.com/ds/2N/2N3904.pdf		
	Diode	Fairchild Semiconductor	1N4002
Datasheet	http://www.fairchildsemi.com/ds/1N/1N4002.pdf		
	DAC	National Instruments	NI-USB 6008
Datasheet	http://sine.ni.com/ds/app/doc/p/id/ds-218/lang/en		

A.5 Monitoring System

	Part	Manufacturer	Part Number
	DAQ	National Instruments	NI-USB 6008
Datasheet	http://sine.ni.com/ds/app/doc/p/id/ds-218/lang/en		
	DAQ	National Instruments	NI-USB 6211
Datasheet	http://sine.ni.com/ds/app/doc/p/id/ds-9/lang/en		
	Transformer	Zettler Magnetics	AHI02512
Datasheet	http://www.alliedelec.com/images/products/datasheets/bm/ZETTLER_MAGNETICS/70037377.pdf		
	Current Sensor	Allegro Microsystems	ACS756KCA-050B-PFF-T
Datasheet	http://www.allegromicro.com/en/Products/Part_Numbers/0756/0756.pdf		
	Varistor	EPCOS Inc.	S07K385
Datasheet	http://www.epcos.com/inf/70/db/var_08/SIOV_Leaded_StandarD.pdf		
	Fuse	Littelfuse Inc.	0251.062MXL
Datasheet	http://www.littelfuse.com/data/en/Data_Sheets/Littelfuse_251_253.pdf		

	Part	Manufacturer	Part Number
	Terminal Block Connector	TE Connectivity	796949-7
Datasheet	http://www.te.com/catalog/pn/en/796949-7		
	Terminal Block Connector	TE Connectivity	796949-2
Datasheet	http://www.te.com/catalog/pn/en/796949-2		
	Terminal Block Connector	TE Connectivity	796949-4
Datasheet	http://www.te.com/catalog/pn/en/796949-4		